COVID-19 pandemic dynamics in South Africa and epidemiological characteristics of three variants of concern (Beta, Delta, and Omicron)

Wan Yang[1*] and Jeffrey Shaman[2]

[1]Department of Epidemiology, [2]Department of Environmental Health Sciences, Mailman School of Public Health, Columbia University, New York, NY, USA

*Correspondence to: wy2202@cumc.columbia.edu

Abstract

Severe acute respiratory syndrome coronavirus 2 (SARS-CoV-2) variants of concern (VOCs) have been key drivers of new coronavirus disease 2019 (COVID-19) pandemic waves. To better understand variant epidemiologic characteristics, here we apply a model-inference system to reconstruct SARS-CoV-2 transmission dynamics in South Africa, a country that has experienced three VOC pandemic waves (i.e. Beta, Delta, and Omicron). We estimate key epidemiologic quantities in each of the nine South African provinces during March 2020 – Feb 2022, while accounting for changing detection rates, infection seasonality, nonpharmaceutical interventions, and vaccination. Model validation shows that estimated underlying infection rates and key parameters (e.g., infection-detection rate and infection-fatality risk) are in line with independent epidemiological data and investigations. In addition, retrospective predictions capture pandemic trajectories beyond the model training period. These detailed, validated model-inference estimates thus enable quantification of both the immune erosion potential and transmissibility of three major SARS-CoV-2 VOCs, i.e., Beta, Delta, and Omicron. These findings help elucidate changing COVID-19 dynamics and inform future public health planning.

Keywords: COVID-19, SARS-CoV-2, variant of concern, immune evasion, transmissibility

INTRODUCTION

Since its emergence in late December 2019, the severe acute respiratory syndrome coronavirus 2 (SARS-CoV-2) has spread globally, causing the coronavirus disease 2019 (COVID-19) pandemic (1). In just two years, SARS-CoV-2 has caused several pandemic waves in quick succession in many places. Many of these repeated pandemic waves have been driven by new variants of concern (VOCs) or interest (VOIs) that erode prior immunity from either infection or vaccination, increase transmissibility, or a combination of both. However, while laboratory and field studies have provided insights into these epidemiological characteristics, quantifying the extent of immune erosion (or evasion) and changes to transmissibility for each VOC remains challenging.

Like many places, by February 2022 South Africa had experienced four distinct pandemic waves caused by the ancestral SARS-CoV-2 and three VOCs (Beta, Delta, and Omicron BA.1). However, South Africa is also unique in that the country had the earliest surge for two of the five VOCs identified to date – namely, Beta (2) and Omicron (3). To better understand the COVID-19 dynamics in South Africa and variant epidemiological characteristics, here we utilize a model-inference system similar to one developed for study of SARS-CoV-2 VOCs, including the Beta variant in South Africa (4). We use this system to reconstruct SARS-CoV-2 transmission dynamics in each of the nine provinces of South Africa from the pandemic onset during March 2020 to the end of February 2022 while accounting for multiple factors modulating underlying transmission dynamics. We then rigorously validate the model-inference estimates using independent data and retrospective predictions. The validated estimates quantify the immune erosion potential and transmissibility of three major SARS-CoV-2 variants, i.e., Beta, Delta, and Omicron (BA.1), in South Africa. Our findings highlight several common characteristics of SARS-CoV-2 VOCs and the need for more proactive planning and preparedness for future VOCs, including development of a universal vaccine that can effectively block SARS-CoV-2 infection as well as prevent severe disease.

RESULTS

Model fit and validation

The model-inference system uses case and death data to reconstruct the transmission dynamics of SARS-CoV-2, while accounting for under-detection of infection, infection seasonality, implemented nonpharmaceutical interventions (NPIs), and vaccination (see Methods). Overall, the model-inference system is able to fit weekly case and death data in each of the nine South African provinces (Fig 1A, Fig S1, and additional discussion in Supplemental Materials). Additional testing (in particular, for the infection-detection rate) and visual inspections indicate that posterior estimates for the model parameters are consistent with those reported in the literature, or changed over time and/or across provinces in directions as would be expected (see Supplemental Materials).

We then validated the model-inference estimates using three independent datasets. First, we used serology data. We note that early in the pandemic serology data may reflect underlying infection rates but later, due to waning antibody titers and reinfection, likely underestimate infection. Compared to seroprevalence measures taken at multiple time points in each province, our model estimated cumulative infection rates roughly match corresponding serology measures and trends over time; as expected, model estimates were higher than serology measures taken during later months (Fig 1B). Second, compared to hospital admission data, across the nine provinces, model estimated infection numbers were well correlated with

numbers of hospitalizations for all four pandemic waves caused by the ancestral, Beta, Delta, and Omicron (BA.1) variants, respectively ($r > 0.75$, Fig S2 A-D). Third, model-estimated infection numbers were correlated with age-adjusted excess mortality for both the ancestral and Delta wave ($r = 0.86$ and 0.61, respectively; Fig S2 A and C). For the Beta wave, after excluding Western Cape, a province with a very high hospitalization rate but low excess mortality during this wave (Fig S2 B), model-estimated infection numbers were also correlated with age-adjusted excess mortality for the remaining provinces ($r = 0.55$; Fig S2 B). For the Omicron (BA.1) wave, like many other places, due to prior infection and/or vaccination (5, 6), mortality rates decoupled from infection rates (Fig S2 D). Overall, comparisons with the three independent datasets indicate our model-inference estimates align with underlying transmission dynamics.

In addition, as a fourth model validation, we generated retrospective predictions of the Delta and Omicron (BA.1) waves at two key time points, i.e. 2 weeks and 1 week, separately, before the observed peak of cases (approximately 3 to 5 weeks before the observed peak of deaths; Fig 2). To accurately predict a pandemic wave caused by a new variant, the model-inference system needs to accurately estimate the background population characteristics (e.g., population susceptibility) before the emergence of the new variant, as well as changes in population susceptibility and transmissibility due to the new variant. This is particularly challenging for South Africa, as the pandemic waves there tended to progress quickly, with cases surging and peaking within 3 to 7 weeks before declining. As a result, often only 1 to 6 weeks of new variant data were available for model-inference before generating the prediction. Despite these challenges, 1-2 weeks before the case peak and 3-5 weeks before the observed death peak, the model was able to accurately predict the remaining trajectories of cases and deaths in most of the nine provinces for both the Delta and Omicron (BA.1) waves (Fig 2 for the four most populous provinces and Fig S3 for the remainder). These accurate model predictions further validate the model-inference estimates.

Pandemic dynamics and key model-inference, using Gauteng province as an example

Next, we use Gauteng, the province with the largest population, as an example to highlight pandemic dynamics in South Africa thus far and develop key model-inference estimates (Fig 3 for Gauteng and Figs S4-S11 for each of the other eight provinces). Despite lower cases per capita than many other countries, infection numbers in South Africa were likely much higher due to under-detection. For Gauteng, the estimated infection-detection rate during the first pandemic wave was 4.59% (95% CI: 2.62 – 9.77%), and increased slightly to 6.18% (95% CI: 3.29 – 11.11%) and 6.27% (95% CI: 3.44 – 12.39%) during the Beta and Delta waves, respectively (Table S1). These estimates are in line with serology data. In particular, a population-level sero-survey in Gauteng found 68.4% seropositivity among those unvaccinated at the end of the Delta

wave (7). Combining the reported cases at that time (~6% of the population size) with undercounting of infections in sero-surveys due to sero-reversions and reinfections suggests that the overall detection rate would be less than 10%.

Using our inferred under-detection (Fig 3E), we estimate that 32.83% (95% CI: 15.42 - 57.59%, Table S2) of the population in Gauteng were infected during the first wave, predominantly during winter when more conducive climate conditions and relaxed public health restrictions existed (see the estimated seasonal and mobility trends, Fig 3A). This high infection rate, while with uncertainty, is in line with serology measures taken in Gauteng at the end of the first wave (ranging from 15% to 27% among 6 sero-surveys during November 2020; Fig 1B) and a study showing 30% sero-positivity among participants enrolled in the Novavax NVX-CoV2373 vaccine phase 2a-b trial in South Africa during August – November 2020 (8).

With the emergence of Beta, another 21.87% (95% CI: 12.16 – 41.13%) of the population in Gauteng – including reinfections – is estimated to have been infected, even though the Beta wave occurred during summer under less conducive climate conditions for transmission (Fig 3A). The model-inference system estimates a large increase in population susceptibility with the surge of Beta (Fig 3D; note population susceptibility is computed as S / N × 100%, where S is the estimated number of susceptible people and N is population size). This dramatic increase in population susceptibility (vs. a likely more gradual change due to waning immunity), to the then predominant Beta variant, suggests Beta likely substantially eroded prior immunity and is consistent with laboratory studies showing low neutralizing ability of convalescent sera against Beta (9, 10). In addition, an increase in transmissibility is also evident for Beta, after accounting for concurrent NPIs and infection seasonality (Fig 3C; note transmissibility is computed as the product of the estimated variant-specific transmission rate and the infectious period; see Methods for detail). Notably, in contrast to the large fluctuation of the time-varying effective reproduction number over time (R_t, Fig 3B), the transmissibility estimates are more stable and reflect changes in variant-specific properties. Further, consistent with in-depth epidemiological findings (11), the estimated overall infection-fatality risk for Beta was about twice as high as the ancestral SARS-CoV-2 (0.19% [95% CI: 0.10 - 0.33%] vs. 0.09% [95% CI: 0.05 - 0.20%], Fig 3F and Table S3). Nonetheless, these estimates are based on documented COVID-19 deaths and are likely underestimates.

With the introduction of Delta, a third pandemic wave occurred in Gauteng during the 2021 winter. The model-inference system estimates a 49.82% (95% CI: 25.22 – 90.79%) attack rate by Delta, despite the large number of infections during the previous two waves. This large attack rate was possible due to the high transmissibility of Delta, as reported in multiple studies (12-

16), the more conducive winter transmission conditions (Fig 3A), and the immune erosive properties of Delta relative to both the ancestral and Beta variants (17-19).

Due to these large pandemic waves, prior to the detection of Omicron (BA.1) in Gauteng, estimated cumulative infection numbers surpassed the population size (Fig 4B), indicating the large majority of the population had been infected and some more than once. With the rise of Omicron (BA.1), the model-inference system estimates a very large increase in population susceptibility (Fig 3D), as well as an increase in transmissibility (Fig 3C); however, unlike previous waves, the Omicron (BA.1) wave progresses much more quickly, peaking 2-3 weeks after initiating marked exponential growth. These estimates suggest that several additional factors may have also contributed to the observed dynamics, including changes to the infection-detection rate (Fig 3E and Supplemental Materials), a summer seasonality increasingly suppressing transmission as the wave progressed (Fig 3A), as well as a slight change in population mobility suggesting potential behavior changes (Fig 3A). By the end of February 2022, the model-inference system estimates a 44.49% (95% CI: 19.01 – 75.30%) attack rate, with only 4.26% (95% CI: 2.46 – 9.72%) of infections detected as cases, during the Omicron (BA.1) wave in Gauteng. In addition, consistent with the reported 0.3 odds of severe disease compared to Delta infections (6), estimated overall infection-fatality risk during the Omicron (BA.1) wave was about 30% of that during the Delta wave in Gauteng (0.03% [95% CI: 0.02 – 0.06%] vs. 0.11% [95% CI: 0.06 – 0.21%], based on documented COVID-19 deaths; Table S3).

Model inferred epidemiological characteristics across the nine provinces in South Africa

Across all nine provinces in South Africa, the pandemic timing and intensity varied (Fig 4 A-C). In addition to Gauteng, high cumulative infection rates during the first three pandemic waves are also estimated for Western Cape and Northern Cape (Fig 1 C-E, Fig 4B and Table S2). Overall, all nine provinces likely experienced three large pandemic waves prior to the growth of Omicron (BA.1); estimated average cumulative infections ranged from 60% of the population in Limpopo to 122% in Northern Cape (Fig 4B). Corroboration for these cumulative infection estimates is derived from mortality data. Excess mortality before the Omicron (BA.1) wave was as high as 0.47% of the South African population by the end of November 2021 (20), despite the relatively young population (median age: 27.6 years (21) vs. 38.5 years in the US (22)) and thus lower expected infection-fatality risk (23, 24). Assuming an infection-fatality risk of 0.5% (similar to estimates in (25) for South Africa), these excess deaths would convert to a 94% infection rate.

We then use these model-inference estimates to quantify the immune erosion potential and increase in transmissibility for each VOC. Specifically, the immune erosion (against infection) potential is computed as the ratio of two quantities – the numerator is the increase of

population susceptibility due to a given VOC and the denominator is population immunity (i.e., complement of population susceptibility) at wave onset. The relative increase in transmissibility is also computed as a ratio, i.e., the average increase due to a given VOC relative to the ancestral SARS-CoV-2 (see Methods). As population-specific factors contributing to transmissibility (e.g., population density and average contact rate) would be largely cancelled out in the latter ratio, we expect estimates of the VOC transmissibility increase to be generally applicable to different populations. However, prior exposures and vaccinations varied over time and across populations; thus, the level of immune erosion is necessarily estimated relative to the local population immune landscape at the time of the variant surge and should be interpreted accordingly. In addition, this assessment does not distinguish the sources of immunity or partial protection against severe disease; rather, it assesses the overall loss of immune protection against infection for a given VOC.

In the above context, we estimate that Beta eroded immunity among 63.4% (95% CI: 45.0 – 77.9%) of individuals with prior ancestral SARS-CoV-2 infection and was 34.3% (95% CI: 20.5 – 48.2%) more transmissible than the ancestral SARS-CoV-2. These estimates for Beta are consistent across the nine provinces (Fig 4D, 1st column and Table 1), as well as with our previous estimates using national data for South Africa (4). Additional support for the high immune erosion of Beta is evident from recoverees of ancestral SARS-CoV-2 infection who were enrolled in the Novavax NVX-CoV2373 vaccine phase 2a-b trial (8) and found to have a similar likelihood of COVID-19, mostly due to Beta, compared to those seronegative at enrollment.

Estimates for Delta vary across the nine provinces (Fig 4D, 2nd column), given the more diverse population immune landscape among provinces after two pandemic waves. Overall, we estimate that Delta eroded 24.5% (95% CI: 0 – 53.2%) of prior immunity (gained from infection by ancestral SARS-CoV-2 and/or Beta, and/or vaccination) and was 47.5% (95% CI: 28.4 – 69.4%) more transmissible than the ancestral SARS-CoV-2. Consistent with this finding, and in particular the estimated immune erosion, studies have reported a 27.5% reinfection rate during the Delta pandemic wave in Delhi, India (17) and reduced ability of sera from Beta-infection recoverees to neutralize Delta (18, 19).

For Omicron (BA.1), estimates also vary by province but still consistently point to its higher transmissibility than all previous variants (Fig 4D, 3rd column). Overall, we estimate that Omicron (BA.1) is 94.0% (95% CI: 73.5 – 121.5%) more transmissible than the ancestral SARS-CoV-2. This estimated transmissibility is higher than Delta and consistent with *in vitro* and/or *ex vivo* studies showing Omicron (BA.1) replicates faster within host than Delta (26, 27). In addition, we estimate that Omicron (BA.1) eroded 54.1% (95% CI: 35.8 – 70.1%) of immunity due to all prior infections and vaccination. Importantly, as noted above, the estimate for

immune erosion is not directly comparable across variants, as it is relative to the combined population immunity accumulated until the rise of each variant. In the case of Beta, it is immunity accumulated from the first wave via infection by the ancestral SARS-CoV-2. In the case of Omicron (BA.1), it includes immunity from prior infection and refection of any of the previously circulating variants as well as vaccination. Thus, the estimate for Omicron (BA.1) may represent a far broader capacity for immune erosion than was evident for Beta. Supporting the suggestion of broad-spectrum immune erosion of Omicron (BA.1), studies have reported low neutralization ability of convalescent sera from infections by all previous variants (28, 29), as well as high attack rates among vaccinees in several Omicron (BA.1) outbreaks (30, 31).

DISCUSSION

Using a comprehensive model-inference system, we have reconstructed the pandemic dynamics in each of the nine provinces of South Africa. Uncertainties exist in our findings, due to incomplete and varying detection of SARS-CoV-2 infections and deaths, changing population behavior and public health interventions, and changing circulating variants. To address these uncertainties, we have validated our estimates using three datasets not used by our model-inference system (i.e., serology, hospitalization, and excess mortality data; Fig 1B and Fig S2) as well as retrospective prediction (Fig 2 and Fig S4). In addition, as detailed in the Results, we have showed that estimated underlying infection rates (Fig 1B and Fig S2) and key parameters (e.g., infection-detection rate and infection-fatality risk) are in line with other independent epidemiological data and investigations. The detailed, validated model-inference estimates thus allow quantification of both the immune erosion potential and transmissibility of three major SARS-CoV-2 VOCs, i.e., Beta, Delta, and Omicron (BA.1).

The relevance of our model-inference estimates to previous studies has been presented in the Results section. Here, we make three additional general observations, drawn from global SARS-CoV-2 dynamics including but not limited to findings in South Africa. First, high prior immunity does not preclude new outbreaks, as neither infection nor current vaccination is sterilizing. As shown in South Africa, even with the high infection rate accumulated from preceding waves, new waves can occur with the emergence or introduction of new variants. Around half of South Africans are estimated to have been infected after the Beta wave (Table S2 and Table S4), yet the Delta variant caused a third large pandemic wave, followed by a fourth wave with comparable infection rates by Omicron BA.1 (Fig 4B and Table S2).

Second, large numbers of hospitalizations and/or deaths can still occur in later waves with large infection surges, even though prior infection may provide partial protection and to some extent temper disease severity. This is evident from the large Delta wave in South Africa, which resulted in 0.2% excess mortality (vs. 0.08% during the first wave and 0.19% during the Beta

wave (20)). More recently, due to the Omicron BA.4/BA.5 subvariants that have been shown to evade prior immunity including from BA.1 infection (32, 33), a fifth wave began in South Africa during May 2022, leading to increases in both cases and hospitalizations (34). Together, the continued transmission and potential severe outcomes highlight the importance of continued preparedness and prompt public health actions as societies learn to live with SARS-CoV-2.

Third, multiple SARS-CoV-2 VOCs/VOIs have emerged in the two years since pandemic inception. It is challenging to predict the frequency and direction of future viral mutation, in particular, the level of immune erosion, changes in transmissibility, and innate severity. Nonetheless, given high exposure and vaccination in many populations, variants capable of eroding a wide spectrum of prior immunity (i.e., from infection by multiple preexisting variants and vaccination) would have a greater chance of causing new major outbreaks. Indeed, except for the Alpha variant, the other four important VOCs (i.e. Beta, Gamma, Delta, and Omicron) all produced some level of immune erosion. In addition, later VOCs, like Delta and Omicron, appear to have been more genetically distinct from previous variants (35). As a result, they are likely more capable of causing re-infection despite diverse prior exposures and in turn new pandemic waves. Given this pattern, to prepare for future antigenic changes from new variants, development of a universal vaccine that can effectively block SARS-CoV-2 infection in addition to preventing severe disease (e.g. shown in (36)) is urgently needed (37).

The COVID-19 pandemic has caused devastating public health and economic burdens worldwide. Yet SARS-CoV-2 will likely persist in the future. To mitigate its impact, proactive planning and preparedness is paramount.

METHODS

Data sources and processing

We used reported COVID-19 case and mortality data to capture transmission dynamics, weather data to estimate infection seasonality, mobility data to represent concurrent NPIs, and vaccination data to account for changes in population susceptibility due to vaccination in the model-inference system. Provincial level COVID-19 case, mortality, and vaccination data were sourced from the Coronavirus COVID-19 (2019-nCoV) Data Repository for South Africa (COVID19ZA)(38). Hourly surface station temperature and relative humidity came from the Integrated Surface Dataset (ISD) maintained by the National Oceanic and Atmospheric Administration (NOAA) and are accessible using the “stationaRy” R package (39, 40). We computed specific humidity using temperature and relative humidity per the Clausius-Clapeyron equation (41). We then aggregated these data for all weather stations in each province with measurements since 2000 and calculated the average for each week of the year during 2000-2020.

Mobility data were derived from Google Community Mobility Reports (42); we aggregated all business-related categories (i.e., retail and recreational, transit stations, and workplaces) in all locations in each province to weekly intervals. For vaccination, provincial vaccination data from the COVID19ZA data repository recorded the total number of vaccine doses administered over time; to obtain a breakdown for numbers of partial (1 dose of mRNA vaccine) and full vaccinations (1 dose of Janssen vaccine or 2 doses of mRNA vaccine), separately, we used national vaccination data for South Africa from Our World in Data (43, 44) to apportion the doses each day. In addition, cumulative case data suggested 18,586 new cases on Nov 23, 2021, whereas the South Africa Department of Health reported 868 (45). Thus, for Nov 23, 2021, we used linear interpolation to fill in estimates for each province on that day and then scaled the estimates such that they sum to 868.

Model-inference system

The model-inference system is based on our previous work estimating changes in transmissibility and immune erosion for SARS-CoV-2 VOCs including Alpha, Beta, Gamma, and Delta (4, 46). Below we describe each component.

Epidemic model

The epidemic model follows an SEIRSV (susceptible-exposed-infectious-recovered-susceptible-vaccination) construct per Eqn 1:

$$\begin{cases} \dfrac{dS}{dt} = \dfrac{R}{L_t} - \dfrac{b_t e_t m_t \beta_t IS}{N} - \varepsilon - v_{1,t} - v_{2,t} \\ \dfrac{dE}{dt} = \dfrac{b_t e_t m_t \beta_t IS}{N} - \dfrac{E}{Z_t} + \varepsilon \\ \dfrac{dI}{dt} = \dfrac{E}{Z_t} - \dfrac{I}{D_t} \\ \dfrac{dR}{dt} = \dfrac{I}{D_t} - \dfrac{R}{L_t} + v_{1,t} + v_{2,t} \end{cases}$$

where S, E, I, R are the number of susceptible, exposed (but not yet infectious), infectious, and recovered/immune/deceased individuals; N is the population size; and ε is the number of travel-imported infections. In addition, the model includes the following key components:

1) Virus-specific properties, including the time-varying variant-specific transmission rate β_t, latency period Z_t, infectious period D_t, and immunity period L_t. Of note, the immunity period L_t and the term R/L_t in Eqn 1 are used to model the waning of immune protection

against infection. Also note that all parameters are estimated for each week (t) as described below.

2) The impact of NPIs. Specifically, we use relative population mobility (see data above) to adjust the transmission rate via the term m_t, as the overall impact of NPIs (e.g., reduction in the time-varying effective reproduction number R_t) has been reported to be highly correlated with population mobility during the COVID-19 pandemic.(47-49) To further account for potential changes in effectiveness, the model additionally includes a parameter, e_t, to scale NPI effectiveness.

3) The impact of vaccination, via the terms $v_{1,t}$ and $v_{2,t}$. Specifically, $v_{1,t}$ is the number of individuals successfully immunized after the first dose of vaccine and is computed using vaccination data and vaccine effectiveness (VE) for 1st dose; and $v_{2,t}$ is the additional number of individuals successfully immunized after the second vaccine dose (i.e., excluding those successfully immunized after the first dose). In South Africa, around two-thirds of vaccines administered during our study period were the mRNA BioNTech/Pfizer vaccine and one-third the Janssen vaccine (50). We thus set VE to 20%/85% (partial/full vaccination) for Beta, 35%/75% for Delta, and 10%/35% for Omicron (BA.1) based on reported VE estimates (51-53).

4) Infection seasonality, computed using temperature and specific humidity data as described previously (see supplemental material of Yang and Shaman(4)). Briefly, we estimated the relative seasonal trend (b_t) using a model representing the dependency of the survival of respiratory viruses including SARS-CoV-2 to temperature and humidity (54, 55), per

$$R_0(t) = [aq^2(t) + bq(t) + c][\frac{T_c}{T(t)}]^{T_{exp}} \quad \text{(Eqn 2)}$$

$$b_t = \frac{R_0(t)}{\overline{R_0(t)}} \quad \text{(Eqn 3)}$$

In essence, the seasonality function in Eqn 2 assumes that humidity has a bimodal effect on seasonal risk of infection, with both low and high humidity conditions favoring transmission [i.e., the parabola in 1st set of brackets, where $q(t)$ is weekly specific humidity measured by local weather stations]; and this effect is further modulated by temperature, with low temperatures promoting transmission and temperatures above a certain threshold limiting transmission [i.e., 2nd set of brackets, where $T(t)$ is weekly temperature measured by local weather stations and T_c is the threshold]. As SARS-CoV-2 specific parameters (a, b, c, T_c, and T_{exp} in Eqn 2) are not available, to estimate its seasonality using Eqn 2, as done in Yang and Shaman (4), we use parameters estimated for influenza (56) and scale the weekly outputs [i.e., $R_0(t)$] by the annual mean (i.e., $\overline{R_0}$) per Eqn 3. In doing so, the scaled outputs (b_t) are no longer specific to influenza; rather, they represent the *relative*, seasonality-related transmissibility by week, general to viruses sharing similar seasonal responses. As shown in Fig 2A, b_t estimates over the year averaged to 1 such that weeks with b_t >1 (e.g. during the winter) are more conducive to SARS-CoV-2 transmission whereas weeks with b_t

<1 (e.g. during the summer) have less favorable climate conditions for transmission. The estimated relative seasonal trend, b_t, is used to adjust the relative transmission rate at time t in Eqn 1.

Observation model to account for under-detection and delay

Using the model-simulated number of infections occurring each day, we further computed the number of cases and deaths each week to match with the observations, as done in Yang et al (57). Briefly, we include 1) a time-lag from infectiousness to detection (i.e., an infection being diagnosed as a case), drawn from a gamma distribution with a mean of $T_{d,mean}$ days and a standard deviation of $T_{d,sd}$ days, to account for delays in detection (Table S5); 2) an infection-detection rate (r_t), i.e. the fraction of infections (including subclinical or asymptomatic infections) reported as cases, to account for under-detection; 3) a time-lag from infectiousness to death, drawn from a gamma distribution with a mean of 13-15 days and a standard deviation of 10 days; and 4) an infection-fatality risk (IFR_t). To compute the model-simulated number of new cases each week, we multiplied the model-simulated number of new infections per day by the infection-detection rate, and further distributed these simulated cases in time per the distribution of time-from-infectiousness-to-detection. Similarly, to compute the model-simulated deaths per week and account for delays in time to death, we multiplied the simulated-infections by the IFR and then distributed these simulated deaths in time per the distribution of time-from-infectious-to-death. We then aggregated these daily numbers to weekly totals to match with the weekly case and mortality data for model-inference. For each week, the infection-detection rate (r_t), the infection-fatality risk (IFR_t)., and the two time-to-detection parameters ($T_{d,mean}$ and $T_{d,sd}$) were estimated along with other parameters (see below).

Model inference and parameter estimation

The inference system uses the ensemble adjustment Kalman filter (EAKF (58)), a Bayesian statistical method, to estimate model state variables (i.e., S, E, I, R from Eqn 1) and parameters (i.e., β_t, Z_t, D_t, L_t, e_t, from Eqn 1 as well as r_t, IFR_t and other parameters from the observation model). Briefly, the EAKF uses an ensemble of model realizations (n=500 here), each with initial parameters and variables randomly drawn from a *prior* range (see Table S5). After model initialization, the system integrates the model ensemble forward in time for a week (per Eqn 1) to compute the prior distribution for each model state variable and parameter, as well as the model-simulated number of cases and deaths for that week. The system then combines the prior estimates with the observed case and death data for the same week to compute the posterior per Bayes' theorem (58). During this filtering process, the system updates the posterior distribution of all model variables and parameters for each week. For a further discussion on the filtering process and additional considerations, see the Supplemental text;

diagnosis of model posterior estimates for all parameters are also included in the Supplemental text and Figs. S15 – S23.

Estimating changes in transmissibility and immune erosion for each variant

As in ref (4), we computed the variant-specific transmissibility (R_{TX}) as the product of the variant-specific transmission rate (β_t) and infectious period (D_t). Note that R_t, the time-varying effective reproduction number, is defined as $R_t = b_t e_t m_t \beta_t D_t S/N = b_t e_t m_t R_{TX} S/N$. To reduce uncertainty, we averaged transmissibility estimates over the period a particular variant of interest was predominant. To find these predominant periods, we first specified the approximate timing of each pandemic wave in each province based on: 1) when available, genomic surveillance data; specifically, the onsets of the Beta wave in Eastern Cape, Western Cape, KwaZulu-Natal, and Northern Cape, were separately based on the initial detection of Beta in these provinces as reported in Tegally et al. (2); the onsets of the Delta wave in each of the nine provinces, separately, were based on genomic sequencing data from the Network for Genomic Surveillance South Africa (NGS-SA)(59); and 2) when genomic data were not available, we used the week with the lowest case number between two waves. The specified calendar periods are listed in Table S6. During later waves, multiple variants could initially co-circulate before one became predominant. As a result, the estimated transmissibility tended to increase before reaching a plateau (see, e.g., Fig 2C). In addition, in a previous study of the Delta pandemic wave in India (46), we also observed that when many had been infected, transmissibility could decrease a couple months after the peak, likely due to increased reinfections for which onward transmission may be reduced. Thus, to obtain a more variant-specific estimate, we computed the average transmissibility ($\overline{R_{TX}}$) using the weekly R_{TX} estimates over the 8-week period starting the week prior to the maximal R_{tx} during each wave; if no maximum existed (e.g. when a new variant is less transmissible), we simply averaged over the entire wave. We then computed the change in transmissibility due to a given variant relative to the ancestral SARS-CoV-2 as $(\frac{\overline{R_{TX,variant}} - \overline{R_{TX,ancestral}}}{\overline{R_{TX,ancestral}}}) \times 100\%$.

To quantify immune erosion, similar to ref (4), we estimated changes in susceptibility over time and computed the change in immunity as ΔImm = $S_{t+1} - S_t + i_t$, where S_t is the susceptibility at time-t and i_t is the new infections occurring during each week-t. We sum over all ΔImm estimates for a particular location, during each wave, to compute the total change in immunity due to a new variant, $\Sigma\Delta Imm_v$. Because filter adjustment could also slightly increase S, to avoid overestimation, here we only included substantial increases (i.e., ΔImm per week > 0.5% of the total population) when computing changes due to a new variant. As such, we did not further account for smaller susceptibility increases due to waning immunity [for reference, for a population that is 50% immune and a 2-year mean immunity period, 0.5 / (52 × 2) × 100% =

0.48% of the population would lose immunity during a week due to waning immunity]. We then computed the level of immune erosion as the ratio of $\Sigma\Delta Imm_v$ to the model-estimated population immunity prior to the first detection of immune erosion, during each wave. That is, as opposed to having a common reference of prior immunity, here immune erosion for each variant depends on the state of the population immune landscape – i.e., combining all prior exposures and vaccinations – immediately preceding the surge of that variant.

For all provinces, model-inference was initiated the week starting March 15, 2020 and run continuously until the week starting February 27, 2022. To account for model stochasticity, we repeated the model-inference process 100 times for each province, each with 500 model realizations and summarized the results from all 50,000 model estimates.

Model validation using independent data

To compare model estimates with independent observations not assimilated into the model-inference system, we utilized three relevant datasets:

1) Serological survey data measuring the prevalence of SARS-CoV-2 antibodies over time. Multiple serology surveys have been conducted in different provinces of South Africa. The South African COVID-19 Modelling Consortium summarizes the findings from several of these surveys (see Fig 1A of ref (60)). We digitized all data presented in Fig 1A of ref (60) and compared these to corresponding model-estimated cumulative infection rates (computed mid-month for each corresponding month with a seroprevalence measure). Due to unknown survey methodologies and challenges adjusting for sero-reversion and reinfection, we used these data directly (i.e., without adjustment) for qualitative comparison.
2) COVID-19-related hospitalization data, from COVID19ZA (38). We aggregated the total number of COVID-19 hospital admissions during each wave and compared these aggregates to model-estimated cumulative infection rates during the same wave. Of note, these hospitalization data were available from June 6, 2020 onwards and are thus incomplete for the first wave.
3) Age-adjusted excess mortality data from the South African Medical Research Council (SAMRC)(20). Deaths due to COVID-19 (used in the model-inference system) are undercounted. Thus, we also compared model-estimated cumulative infection rates to age-adjusted excess mortality data during each wave. Of note, excess mortality data were available from May 3, 2020 onwards and are thus incomplete for the first wave.

Model validation using retrospective prediction

As a fourth model validation, we generated model predictions at 2 or 1 week before the week of highest cases for the Delta and Omicron (BA.1) waves, separately, and compared the

predicted cases and deaths to reported data unknown to the model. Predicting the peak timing, intensity, and epidemic turnaround requires accurate estimation of model state variables and parameters that determine future epidemic trajectories. This is particularly challenging for South Africa as the pandemic waves tended to progress quickly such that cases surged to a peak in only 3 to 7 weeks. Thus, we chose to generate retrospective predictions 2 and 1 weeks before the peak of cases in order to leverage 1 to 6 weeks of new variant data for estimating epidemiological characteristics. Specifically, for each pandemic wave, we ran the model-inference system until 2 weeks (or 1 week) before the observed peak of cases, halted the inference, and used the population susceptibility and transmissibility of the circulating variant estimated at that time to predict cases and deaths for the remaining weeks (i.e. 10-14 weeks into the future). Because the infection detection rate and fatality risk are linked to observations of cases and deaths, changes of these quantities during the prediction period could obscure the underlying infection rate and accuracy of the prediction. Thus, for these two parameters specifically, we used model-inference estimates for corresponding weeks to allow comparison of model-predicted cases and deaths with the data while focusing on testing the accuracy of other key model estimates (e.g., transmissibility of the new variant). As for the model-inference, we repeated each prediction 100 times, each with 500 model realizations and summarized the results from all 50,000 ensemble members.

Data Availability: All data used in this study are publicly available as described in the "Data sources and processing" section.

Code availability: All source code and data necessary for the replication of our results and figures are publicly available at https://github.com/wan-yang/covid_SouthAfrica.

Acknowledgements: This study was supported by the National Institute of Allergy and Infectious Diseases (AI145883 and AI163023), the Centers for Disease Control and Prevention (CK000592), and a gift from the Morris-Singer Foundation.

Author contributions: WY designed the study (main), conducted the model analyses, interpreted results, and wrote the first draft. JS designed the study (supporting), interpreted results, and critically revised the manuscript.

Competing interests: JS and Columbia University disclose partial ownership of SK Analytics. JS discloses consulting for BNI.

References:

1. Koelle K, Martin MA, Antia R, Lopman B, & Dean NE (2022) The changing epidemiology of SARS-CoV-2. *Science* 375(6585):1116-1121.
2. Tegally H*, et al.* (2021) Detection of a SARS-CoV-2 variant of concern in South Africa. *Nature* 592(7854):438-443.
3. Viana R*, et al.* (2022) Rapid epidemic expansion of the SARS-CoV-2 Omicron variant in southern Africa. *Nature*.
4. Yang W & Shaman J (2021) Development of a model-inference system for estimating epidemiological characteristics of SARS-CoV-2 variants of concern. *Nature Communications* 12:5573.
5. Nyberg T*, et al.* (Comparative analysis of the risks of hospitalisation and death associated with SARS-CoV-2 omicron (B.1.1.529) and delta (B.1.617.2) variants in England: a cohort study. *The Lancet*.
6. Wolter N*, et al.* (2022) Early assessment of the clinical severity of the SARS-CoV-2 omicron variant in South Africa: a data linkage study. *The Lancet* 399(10323):437-446.
7. Madhi SA*, et al.* (2022) Population Immunity and Covid-19 Severity with Omicron Variant in South Africa. *N Engl J Med* 386(14):1314-1326.
8. Shinde V*, et al.* (2021) Efficacy of NVX-CoV2373 Covid-19 Vaccine against the B.1.351 Variant. *N Engl J Med* 384(20):1899-1909.
9. Garcia-Beltran WF*, et al.* (2021) Multiple SARS-CoV-2 variants escape neutralization by vaccine-induced humoral immunity. *Cell* 184(9):2372-2383 e2379.
10. Wall EC*, et al.* (2021) Neutralising antibody activity against SARS-CoV-2 VOCs B.1.617.2 and B.1.351 by BNT162b2 vaccination. *Lancet*.
11. Abu-Raddad LJ*, et al.* (2021) Severity, Criticality, and Fatality of the Severe Acute Respiratory Syndrome Coronavirus 2 (SARS-CoV-2) Beta Variant. *Clinical Infectious Diseases*.
12. Public Health England (2021) SARS-CoV-2 variants of concern and variants under investigation in England. Technical briefing 14.
13. Allen H*, et al.* (2021) Household transmission of COVID-19 cases associated with SARS-CoV-2 delta variant (B.1.617.2): national case-control study. *The Lancet regional health. Europe*:100252.
14. Challen R*, et al.* (2021) Early epidemiological signatures of novel SARS-CoV-2 variants: establishment of B.1.617.2 in England. *medRxiv*:2021.2006.2005.21258365.
15. Earnest R*, et al.* (2021) Comparative transmissibility of SARS-CoV-2 variants Delta and Alpha in New England, USA. *medRxiv*.
16. Vohringer HS*, et al.* (2021) Genomic reconstruction of the SARS-CoV-2 epidemic in England. *Nature*.
17. Dhar MS*, et al.* (2021) Genomic characterization and epidemiology of an emerging SARS-CoV-2 variant in Delhi, India. *Science*:eabj9932.
18. Liu C*, et al.* (2021) Reduced neutralization of SARS-CoV-2 B.1.617 by vaccine and convalescent serum. *Cell* 184(16):4220-+.
19. de Oliveira T & Lessells R (2021) Update on Delta and other variants in South Africa and other world.
20. The South African Medical Research Council (SAMRC) (2021) Report on Weekly Deaths in South Africa.

21. Anonymous (South Africa Population (live).
22. United States Census Bureau (2020) Census Bureau Releases 2020 Demographic Analysis Estimates.
23. Levin AT*, et al.* (2020) Assessing the age specificity of infection fatality rates for COVID-19: systematic review, meta-analysis, and public policy implications. *Eur J Epidemiol* 35(12):1123-1138.
24. O'Driscoll M*, et al.* (2021) Age-specific mortality and immunity patterns of SARS-CoV-2. *Nature* 590(7844):140-145.
25. Anonymous (Variation in the COVID-19 infection-fatality ratio by age, time, and geography during the pre-vaccine era: a systematic analysis. *The Lancet*.
26. Garcia-Beltran WF*, et al.* (2022) mRNA-based COVID-19 vaccine boosters induce neutralizing immunity against SARS-CoV-2 Omicron variant. *Cell* 185(3):457-466.e454.
27. Hui KPY*, et al.* (2022) SARS-CoV-2 Omicron variant replication in human bronchus and lung ex vivo. *Nature*.
28. Rössler A, Riepler L, Bante D, von Laer D, & Kimpel J (2022) SARS-CoV-2 Omicron Variant Neutralization in Serum from Vaccinated and Convalescent Persons. *New England Journal of Medicine* 386(7):698-700.
29. Cele S*, et al.* (2022) Omicron extensively but incompletely escapes Pfizer BNT162b2 neutralization. *Nature* 602(7898):654-656.
30. Brandal LT*, et al.* (2021) Outbreak caused by the SARS-CoV-2 Omicron variant in Norway, November to December 2021. *Eurosurveillance* 26(50):2101147.
31. Helmsdal G*, et al.* (2022) Omicron outbreak at a private gathering in the Faroe Islands, infecting 21 of 33 triple-vaccinated healthcare workers. *Clinical Infectious Diseases*.
32. Cao Y*, et al.* (2022) BA.2.12.1, BA.4 and BA.5 escape antibodies elicited by Omicron infection. *Nature*.
33. Khan K*, et al.* (2022) Omicron sub-lineages BA.4/BA.5 escape BA.1 infection elicited neutralizing immunity. *medRxiv*:2022.2004.2029.22274477.
34. Sarah Neville, Burn-Murdoch J, & Smyth J (2022) Covid hospital admissions rise in Europe as sub-variants fuel new wave.
35. van der Straten K*, et al.* (2022) Mapping the antigenic diversification of SARS-CoV-2. *medRxiv*:2022.2001.2003.21268582.
36. Mao T*, et al.* (2022) Unadjuvanted intranasal spike vaccine booster elicits robust protective mucosal immunity against sarbecoviruses. *bioRxiv*:2022.2001.2024.477597.
37. Morens DM, Taubenberger JK, & Fauci AS (2021) Universal Coronavirus Vaccines — An Urgent Need. *New England Journal of Medicine* 386(4):297-299.
38. Data Science for Social Impact Research Group at University of Pretoria (2021) Coronavirus COVID-19 (2019-nCoV) Data Repository for South Africa.
39. Iannone R (2020) Package 'stationaRy'.
40. Iannone R (2020) stationaRy.
41. Wallace J & Hobbs P (2006) *Atmospheric Science: An Introductory survey* (Academic Press, New York) 2nd Edition Ed p 504.
42. Google Inc. (2020) Community Mobility Reports.
43. Anonymous (2020) Data on COVID-19 (coronavirus) vaccinations by Our World in Data.

44. Mathieu E*, et al.* (2021) A global database of COVID-19 vaccinations. *Nat Hum Behav* 5(7):947-953.
45. Department of Health Republic of South Africa (2021) Update on Covid-19 (Tuesday 23 November 2021).
46. Yang W & Shaman J (2022) COVID-19 pandemic dynamics in India, the SARS-CoV-2 Delta variant and implications for vaccination. *J R Soc Interface* 19(191):20210900.
47. Yang W, Shaff J, & Shaman J (2021) Effectiveness of non-pharmaceutical interventions to contain COVID-19: a case study of the 2020 spring pandemic wave in New York City. *J R Soc Interface* 18(175):20200822.
48. Lasry A*, et al.* (2020) Timing of Community Mitigation and Changes in Reported COVID-19 and Community Mobility - Four U.S. Metropolitan Areas, February 26-April 1, 2020. *MMWR. Morbidity and mortality weekly report* 69(15):451-457.
49. Kraemer MUG*, et al.* (2020) The effect of human mobility and control measures on the COVID-19 epidemic in China. *Science* 368(6490):493-497.
50. Department of Health Republic of South Africa (2021) Latest Vaccine Statistics.
51. Abu-Raddad LJ, Chemaitelly H, Butt AA, & National Study Group for C-V (2021) Effectiveness of the BNT162b2 Covid-19 Vaccine against the B.1.1.7 and B.1.351 Variants. *N Engl J Med* 385(2):187-189.
52. Bernal JL*, et al.* (2021) Effectiveness of Covid-19 Vaccines against the B.1.617.2 (Delta) Variant. *New England Journal of Medicine* 385(7):585-594.
53. Andrews N*, et al.* (2021) Effectiveness of COVID-19 vaccines against the Omicron (B.1.1.529) variant of concern. *medRxiv*:2021.2012.2014.21267615.
54. Biryukov J*, et al.* (2020) Increasing Temperature and Relative Humidity Accelerates Inactivation of SARS-CoV-2 on Surfaces. *mSphere* 5(4):e00441-00420.
55. Morris DH*, et al.* (2021) Mechanistic theory predicts the effects of temperature and humidity on inactivation of SARS-CoV-2 and other enveloped viruses. *Elife* 10.
56. Yuan H, Kramer SC, Lau EHY, Cowling BJ, & Yang W (2021) Modeling influenza seasonality in the tropics and subtropics. *PLoS Comput Biol* 17(6):e1009050.
57. Yang W*, et al.* (2021) Estimating the infection-fatality risk of SARS-CoV-2 in New York City during the spring 2020 pandemic wave: a model-based analysis. *The Lancet. Infectious diseases* 21(2):203-212.
58. Anderson JL (2001) An ensemble adjustment Kalman filter for data assimilation. *Mon. Weather Rev.* 129(12):2884-2903.
59. The National Institute for Communicable Diseases (NICD) of the National Health Laboratory (NHLS) on behalf of the Network for Genomics Surveillance in South Africa (NGS-SA) (2021) Network for Genomic Surveillance South Africa (NGS-SA) SARS-CoV-2 Sequencing Update 19 August 2021.
60. The South African COVID-19 Modelling Consortium (2021) COVID-19 modelling update: Considerations for a potential fourth wave (17 Nov 2021).

Figure Legends:

Fig 1. Pandemic dynamics in South Africa, model-fit and validation using serology data. (A) Pandemic dynamics in each of the nine provinces (see legend); dots depict reported weekly numbers of cases and deaths; lines show model mean estimates (in the same color). (B) For validation, model estimated infection rates are compared to seroprevalence measures over time from multiple sero-surveys summarized in ref 60. Boxplots depict the estimated distribution for each province (middle bar = mean; edges = 50% CrIs) and whiskers (95% CrIs). Red dots show corresponding measurements. Note that reported mortality was high in February 2022 in some provinces (see additional discussion in Supplemental Materials).

Fig 2. Model validation using retrospective prediction. Model-inference was trained on cases and deaths data since March 15, 2020 until 2 weeks (1st plot in each panel) or 1 week (2nd plot) before the Delta or Omicron (BA.1) wave (see timing on the x-axis); the model was then integrated forward using the estimates made at the time to predict cases (left panel) and deaths (right panel) for the remaining weeks of each wave. Blue lines and surrounding shades show model fitted cases and deaths for weeks before the prediction (line = median, dark blue area = 50% CrIs, and light blue = 80% CrIs). Red lines show model projected median weekly cases and deaths; surrounding shades show 50% (dark red) and 80% (light red) CIs of the prediction. For comparison, reported cases and deaths for each week are shown by the black dots; however, those to the right of the vertical dash lines (showing the start of each prediction) were not used in the model. For clarity, here we show 80% CIs (instead of 95% CIs, which tend to be wider for longer-term projections) and predictions for the four most populous provinces (Gauteng in A and B; KwaZulu-Natal in C and D; Western Cape in E and F; and Eastern Cape in G and H). Predictions for the other five provinces are shown in Fig S3.

Fig 3. Example model-inference estimates for Gauteng. (A) Observed relative mobility, vaccination rate, and estimated disease seasonal trend, compared to case and death rates over time. Key model-inference estimates are shown for the time-varying effective reproduction number R_t (B), transmissibility R_{TX} (C), population susceptibility (D, shown relative to the population size in percentage), infection-detection rate (E), and infection-fatality risk (F). Grey shaded areas indicate the approximate circulation period for each variant. In (B) – (F), blue lines and surrounding areas show the estimated mean, 50% (dark) and 95% (light) CrIs; boxes and whiskers show the estimated mean, 50% and 95% CrIs for estimated infection rates. *Note that the transmissibility estimates (R_{TX} in C) have removed the effects of changing population susceptibility, NPIs, and disease seasonality; thus, the trends are more stable than the reproduction number (R_t in B) and reflect changes in variant-specific properties. Also note that infection-fatality risk estimates were based on reported COVID-19 deaths and may not reflect true values due to likely under-reporting of COVID-19 deaths.*

Fig 4. Model-inferred epidemiological properties for different variants across SA provinces. Heatmaps show (A) Estimated mean infection rates by week (x-axis) and province (y-axis), (B) Estimated mean *cumulative* infection numbers relative to the population size in each province,

and (C) Estimated population susceptibility (to the circulating variant) by week and province. (D) Boxplots in the top row show the estimated distribution of increases in transmissibility for Beta, Delta, and Omicron (BA.1), relative to the Ancestral SARS-CoV-2, for each province (middle bar = median; edges = 50% CIs; and whiskers =95% CIs); boxplots in the bottom row show, for each variant, the estimated distribution of immune erosion to all adaptive immunity gained from infection and vaccination prior to that variant. Red lines show the mean across all provinces.

Table 1. Estimated increases in transmissibility and immune erosion potential for Beta, Delta, and Omicron (BA.1). The estimates are expressed in percentage for the median (and 95% CIs). Note that estimated increases in transmissibility for all three variants are relative to the ancestral strain, whereas estimated immune erosion is relative to the composite immunity combining all previous infections and vaccinations accumulated until the surge of the new variant. See main text and Methods for details.

Province	Quantity	Beta	Delta	Omicron (BA.1)
All combined	% Increase in transmissibility	34.3 (20.5, 48.2)	47.5 (28.4, 69.4)	94 (73.5, 121.5)
	% Immune erosion	63.4 (45, 77.9)	24.5 (0, 53.2)	54.1 (35.8, 70.1)
Gauteng	% Increase in transmissibility	42.2 (35.6, 48.3)	51.8 (44.5, 58.7)	112.6 (96.2, 131.8)
	% Immune erosion	65 (57, 72.2)	44.3 (36.4, 54.9)	64.1 (56, 74.2)
KwaZulu-Natal	% Increase in transmissibility	29.7 (22.9, 36.6)	52.5 (44.8, 60.8)	90.6 (77.9, 102.4)
	% Immune erosion	58.1 (48.3, 71.3)	17.3 (1.4, 27.6)	51.1 (39.3, 58.1)
Western Cape	% Increase in transmissibility	23.4 (20.2, 27.4)	55.2 (48.2, 62.7)	86.1 (72.6, 102.6)
	% Immune erosion	68.9 (62.5, 76.4)	41.5 (35.6, 53.5)	61 (55.5, 67.3)
Eastern Cape	% Increase in transmissibility	24.1 (18, 29.7)	50.2 (40.5, 57.4)	78.4 (67.6, 89.2)
	% Immune erosion	54.6 (45.1, 61.2)	24.2 (15.4, 36.2)	45.3 (34.5, 57.2)
Limpopo	% Increase in transmissibility	32.6 (24.9, 39.8)	38.9 (31.5, 50.5)	91.8 (82.6, 102.4)
	% Immune erosion	56.3 (38.4, 76.2)	1.8 (0, 21.2)	42.1 (33.2, 53.2)
Mpumalanga	% Increase in transmissibility	31.2 (25.4, 38.6)	35.3 (24.9, 48.2)	88.6 (72.8, 104.3)
	% Immune erosion	55.6 (39.8, 70)	3.1 (0, 21.7)	45.9 (37.7, 55.7)
North West	% Increase in transmissibility	43.8 (36.9, 52.1)	36.8 (25.6, 47.5)	100 (81.7, 121.1)
	% Immune erosion	67 (58.4, 75.4)	12.4 (0.4, 30.5)	56.6 (48.2, 68.8)
Free State	% Increase in transmissibility	42.7 (35, 49.8)	43.8 (31.9, 52.1)	92.2 (77.4, 106.9)
	% Immune erosion	70 (64.5, 76.2)	27.7 (17.6, 41.6)	57 (49.5, 66.6)
Northern Cape	% Increase in transmissibility	38.6 (32.6, 44.8)	63.1 (50.4, 79.2)	106 (94.7, 119.6)
	% Immune erosion	75 (67.4, 82)	47.9 (40.5, 59.1)	64 (57.3, 72.6)

706 **Fig 1. Pandemic dynamics in South Africa, model-fit and validation using serology data.** (A)
707 Pandemic dynamics in each of the nine provinces (see legend); dots depict reported weekly
708 numbers of cases and deaths; lines show model mean estimates (in the same color). (B) For
709 validation, model estimated infection rates are compared to seroprevalence measures over
710 time from multiple sero-surveys summarized in ref 60. Boxplots depict the estimated
711 distribution for each province (middle bar = mean; edges = 50% CrIs) and whiskers (95% CrIs).
712 Red dots show corresponding measurements. Note that reported mortality was high in
713 February 2022 in some provinces (see additional discussion in Supplemental Materials).

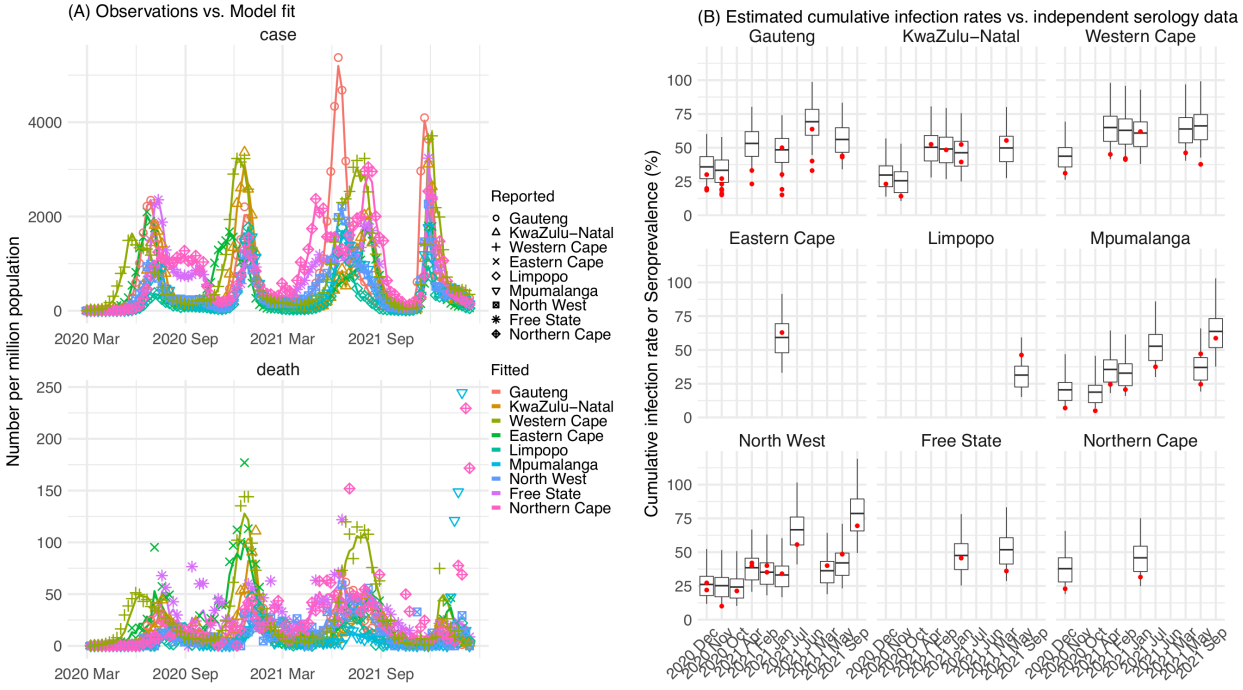

714
715

Fig 2. Model validation using retrospective prediction. Model-inference was trained on cases and deaths data since March 15, 2020 until 2 weeks (1st plot in each panel) or 1 week (2nd plot) before the Delta or Omicron (BA.1) wave (see timing on the x-axis); the model was then integrated forward using the estimates made at the time to predict cases (left panel) and deaths (right panel) for the remaining weeks of each wave. Blue lines and surrounding shades show model fitted cases and deaths for weeks before the prediction (line = median, dark blue area = 50% CrIs, and light blue = 80% CrIs). Red lines show model projected median weekly cases and deaths; surrounding shades show 50% (dark red) and 80% (light red) CIs of the prediction. For comparison, reported cases and deaths for each week are shown by the black dots; however, those to the right of the vertical dash lines (showing the start of each prediction) were not used in the model. For clarity, here we show 80% CIs (instead of 95% CIs, which tend to be wider for longer-term projections) and predictions for the four most populous provinces (Gauteng in A and B; KwaZulu-Natal in C and D; Western Cape in E and F; and Eastern Cape in G and H). Predictions for the other five provinces are shown in Fig S3.

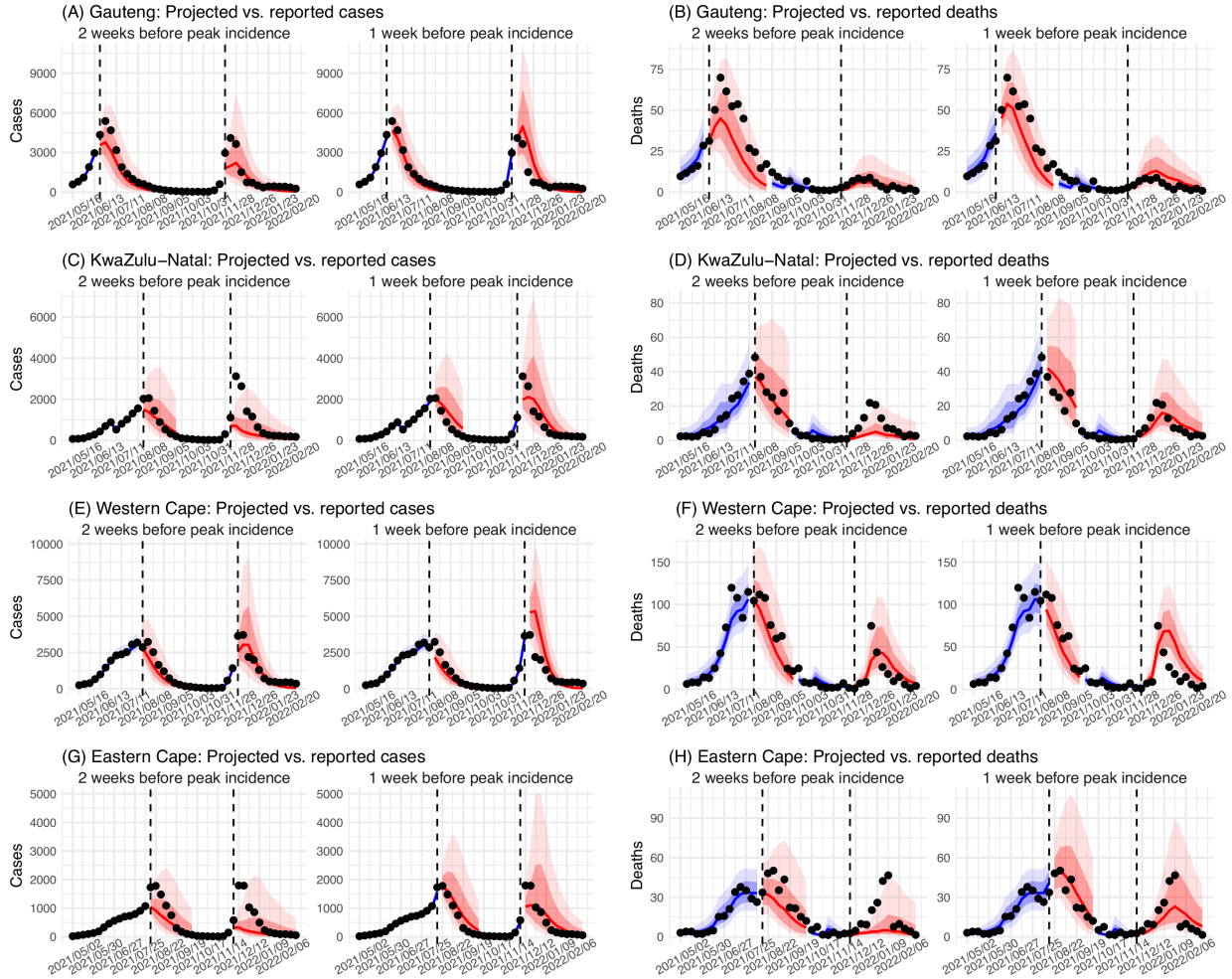

Fig 3. Example model-inference estimates for Gauteng. (A) Observed relative mobility, vaccination rate, and estimated disease seasonal trend, compared to case and death rates over time. Key model-inference estimates are shown for the time-varying effective reproduction number R_t (B), transmissibility R_{TX} (C), population susceptibility (D, shown relative to the population size in percentage), infection-detection rate (E), and infection-fatality risk (F). Grey shaded areas indicate the approximate circulation period for each variant. In (B) – (F), blue lines and surrounding areas show the estimated mean, 50% (dark) and 95% (light) CrIs; boxes and whiskers show the estimated mean, 50% and 95% CrIs for estimated infection rates. *Note that the transmissibility estimates (R_{TX} in C) have removed the effects of changing population susceptibility, NPIs, and disease seasonality; thus, the trends are more stable than the reproduction number (R_t in B) and reflect changes in variant-specific properties. Also note that infection-fatality risk estimates were based on reported COVID-19 deaths and may not reflect true values due to likely under-reporting of COVID-19 deaths.*

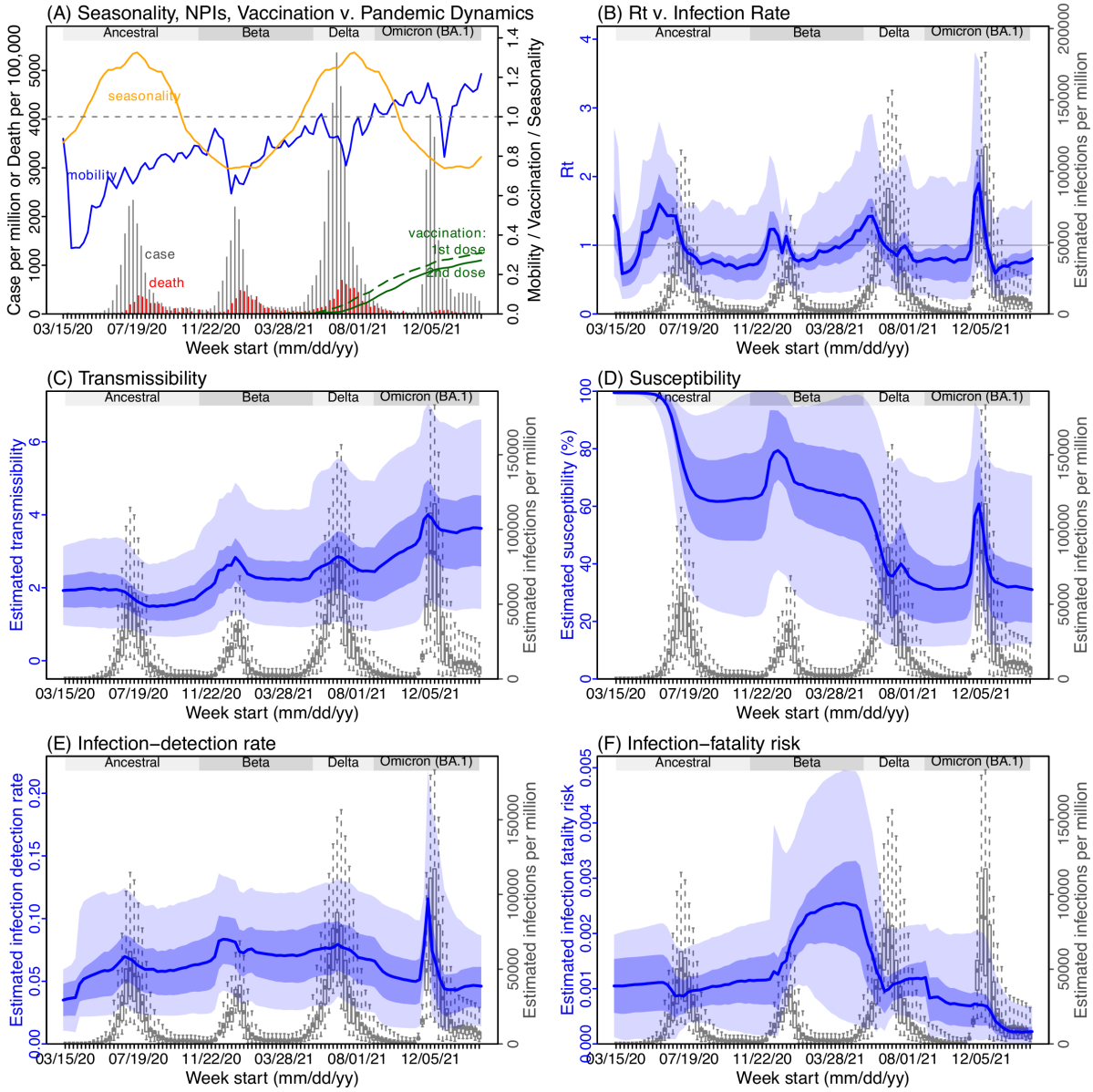

Fig 4. Model-inferred epidemiological properties for different variants across SA provinces. Heatmaps show (A) Estimated mean infection rates by week (x-axis) and province (y-axis), (B) Estimated mean *cumulative* infection numbers relative to the population size in each province, and (C) Estimated population susceptibility (to the circulating variant) by week and province. (D) Boxplots in the top row show the estimated distribution of increases in transmissibility for Beta, Delta, and Omicron (BA.1), relative to the Ancestral SARS-CoV-2, for each province (middle bar = median; edges = 50% CIs; and whiskers =95% CIs); boxplots in the bottom row show, for each variant, the estimated distribution of immune erosion to all adaptive immunity gained from infection and vaccination prior to that variant. Red lines show the mean across all provinces.

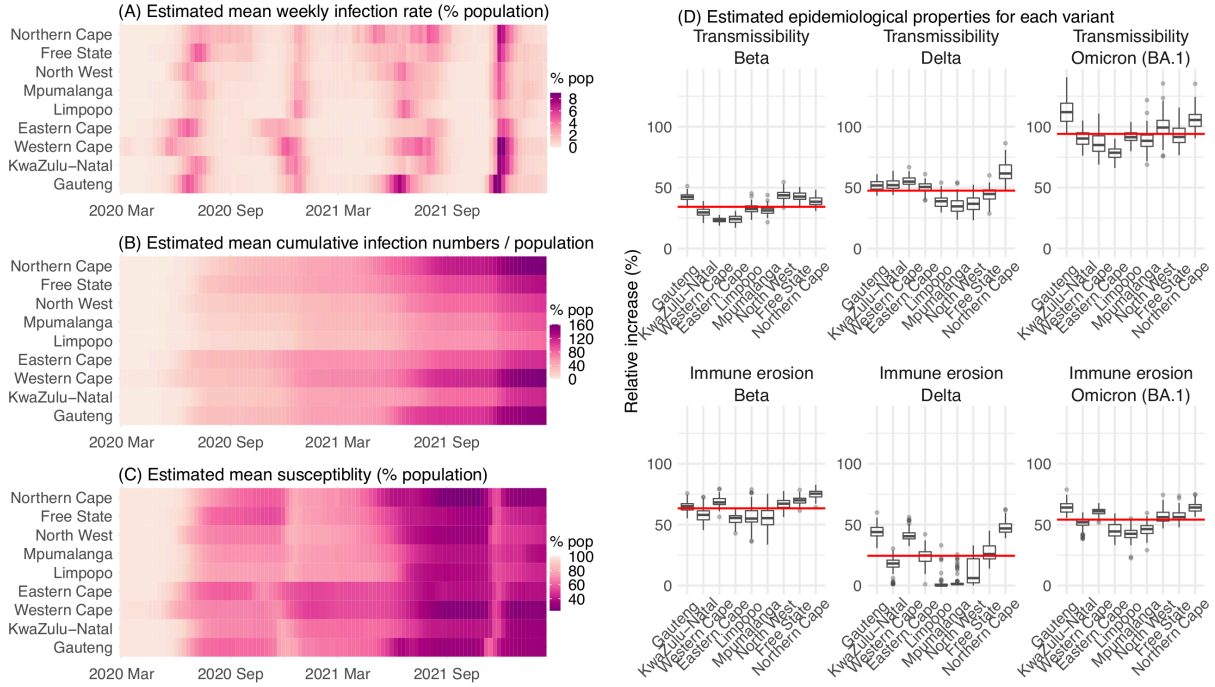

Supplemental Materials

for

COVID-19 pandemic dynamics in South Africa and epidemiological characteristics of three variants of concern (Beta, Delta, and Omicron)

Wan Yang and Jeffrey Shaman

Supplemental results and discussion

1. A brief note on reported COVID-19 mortality and model-inference strategy in this study

COVID-19 mortality data in some South African provinces appeared irregular with very high weekly death counts for some weeks even though cases in preceding weeks were low (see, e.g., COVID-19 related deaths in Mpumalanga and Northern Cape in Fig S1). A likely explanation is the audit and release of mortality data including deaths that occurred in previous time periods, which were not redistributed according to the actual time of death. Such instances have occurred in multiple countries (see, e.g., some of the documentations by Financial Times in ref (1), under the header "SOURCES"). Here, we could not adjust for this possibility due to a lack of information on these apparent data releases. Instead, to account for potential data errors, the ensemble adjustment Kalman filter (EAKF) algorithm (2), used in the model-inference system, includes an estimate of observational error variance for computing the posterior estimates. In this study, the observational error variance was scaled to corresponding observations (thus, weeks with higher mortality would also have larger observational errors). In doing so, the EAKF reduces the weight of observations with larger observational errors (e.g., for weeks with very large death counts), which reduces their impact on the inference of model dynamics. As such, the posterior estimates for mortality tend to (intentionally) miss very high outlying data points (see Fig 1 and Fig S1). In addition, posterior estimates for the infection-fatality risk (IFR) are more stable over time, including for weeks with outlying death counts (see, e.g., Fig S23, IFR estimates for Mpumalanga).

In light of these COVID-19 related mortality data patterns, we computed the overall IFR during each pandemic wave using two methods. The first method computes the wave-specific IFR as the ratio of the total reported COVID-19 related deaths to the model-estimated cumulative infection rate during each wave. Because reported COVID-19 related mortality is used as the numerator, this method is more heavily affected by the aforementioned data irregularities. The second method computes the wave-specific IFR as a weighted average of the weekly IFR estimates during each wave, a measure for which both the numerator and denominator are model-inference derived; the weights are the estimated fraction of infections during each week. As shown in Table S3, for provinces with consistent case and mortality trends (e.g., Gauteng), the two methods generated similar IFR estimates. In contrast, for provinces with

mortality trends inconsistent with case trends (e.g., Mpumalanga), the second method generated IFR estimates more comparable to other provinces than the first method.

2. Considerations in parameter prior choice and the EAKF inference algorithm

The model-inference system included 9 parameters, namely, the variant-specific transmission rate β_t, latency period Z_t, infectious period D_t, immunity period L_t, scaling factor of NPI effectiveness e_t, infection-detection rate r_t, IFR_t, and two parameters for the distribution of time from infectiousness to case detection (i.e., the mean and standard deviation, for a gamma distribution). The initial prior distributions were randomly drawn from uniform distributions with ranges listed in Table S5. For parameters with previous estimates from the literature (e.g., transmission rate β, incubation period Z, infectious period D, and immunity period L; see Table S5, column "Source/rationale"), we set the prior range accordingly. For parameters with high uncertainty and spatial variation (e.g., infection-detection rate), we preliminarily tested initial prior ranges by visualizing model prior and posterior estimates, using different ranges. For instance, for the infection-detection rate, when using a higher prior range (e.g., 5 -20% vs. 1 - 10%), the model prior tended to overestimate observed cases and underestimate deaths. Based on the initial testing, we then used a wide range able to reproduce the observed cases and deaths relatively well and then derived estimates of unobserved state variables and parameters.

Importantly, the EAKF used here is an iterative filtering algorithm. After initialization using the initial prior distributions, it iteratively incorporates additional observations at each time step (here, each week) to compute and update the model posterior (including all model state variables and parameters) using the model prior and the latest observations. For the model state variables, the prior is computed per the dynamic model (here, Eqn 1); for the model parameters, the prior is the posterior from the last time step. As such, the influence of the initial prior range tends to be less pronounced compared to methods such as Markov Chain Monte Carlo (MCMC). In addition, to capture potential changes over time (e.g., likely increased detection for variants causing more severe disease), we applied space reprobing (SR) (3), a technique that randomly replaces parameter values for a small fraction of the model ensemble, to explore a wider range of parameter possibilities (Table S5). Due to both the EAKF algorithm and space reprobing, the posterior parameter estimates can migrate outside the initial parameter ranges (e.g., for the transmission rate during the circulation of new variants).

3. Testing of the infection-detection rate during the Omicron (BA.1) wave in Gauteng

A major challenge for this study is inferring the underlying transmission dynamics of the Omicron (BA.1) wave in Gauteng, where Omicron was initially detected and had the earliest case surge. In Gauteng, the number of cases during the first week of reported detection (i.e.,

the week starting 11/21/21) increased 4.4 times relative to the previous week; during the second week of report (i.e., the week starting 11/28/21) cases increased another 4.9 times. Yet after these two weeks of dramatic increases, cases peaked during the third week and started to decline afterwards. Initial testing suggested substantial changes in infection-detection rates during this time; in particular, detection could increase during the first two weeks due to awareness and concern for the novel Omicron variant and decline during later weeks due to constraints on testing capacity as well as subsequent reports of milder disease caused by Omicron. To more accurately estimate the infection-detection rate and underlying transmission dynamics, we ran and compared model-inference estimates using 4 settings for the infection-detection rate.

As noted above, with the model-EAKF filtering algorithm, parameter posterior is iteratively updated and becomes the prior at the next time step such that information from all previous time steps is sequentially incorporated. Given the sequential nature of the EAKF, rather than using a new prior distribution for the infection-detection rate, to explore new state space (here, potential changes in detection rate), we applied SR (3), which randomly assigns the prior values of a small fraction of the model ensemble while preserving the majority that encodes prior information. In previous studies (3, 4), we have showed that the model ensemble posterior would remain similar if there is no substantial change in the system and more efficiently migrate towards new state space if there is a substantial change. Here, to explore potential changes in infection detection rates during the Omicron (BA.1) wave, we tested 4 SR settings for the infection-detection rate: 1) Use of the same baseline range as before (i.e., 1-8%; uniform distribution, same for other ranges) for all weeks during the Omicron (BA.1) wave; 2) Use of a wider and higher range (i.e., 1-12%) for all weeks; 3) Use of a range of 1-15% for the 1st week of Omicron reporting (i.e., week starting 11/21/21), 5-20% for the 2nd week of Omicron reporting (i.e., the week starting 11/28/21), and 1-8% for the rest; and 4) Use of a range of 5-25% for the 2nd week of reporting and 1-8% for all others.

Estimated infection-detection rates in Gauteng increased substantially during the first two weeks of the Omicron (BA.1) wave and decreased afterwards under all four SR settings (Fig S12, 1st row). This consistency suggests a general trend in infection-detection rates at the time in accordance with the aforementioned potential changes in testing. Without using a higher SR range (e.g., 1-8% and 1-12% in columns 1-2 of Fig S12 vs 5-20% and 5-25% for week 2 in columns 3-4), the estimated increases in infection-detection rate were lower; instead, the model-inference system attributed the dramatic case increases in the first two weeks to higher increases in population susceptibility and transmissibility (Fig S12, 2nd and 3rd row, compare columns 1-2 vs. 3-4). However, the higher estimates for population susceptibility and transmissibility contradicted with the drastic decline in cases shortly afterwards such that the

model-inference system readjusted the transmissibility to a lower level during later weeks (see the uptick in estimated transmissibility in Fig S12, 3rd row, first 2 columns). In contrast, when higher infection-detection rates were estimated for the first two weeks using the last two SR settings, the transmissibility estimates were more stable during later weeks (Fig S12, 3rd row, last 2 columns). In addition, model-inference using the latter two SR settings also generated more accurate retrospective predictions for the Omicron (BA.1) wave in Gauteng (Fig S13).

Given the above results, we used the 4th SR setting in the model-inference for Gauteng (i.e., replace a fraction of the infection detection rate using values randomly drawn from U[5%, 25%] for the week starting 11/28/21 and U[1%, 8%] for all other weeks during the Omicron wave). Reported cases in other provinces did not change as dramatically as in Gauteng; therefore, for those provinces, we used the baseline setting, i.e., values drawn from U[1%, 8%], for re-probing the infection-detection rate. Nonetheless, we note that the overall estimates for changes in transmissibility and immune erosion of Omicron (BA.1) were slightly higher under the first two SR settings but still consistent with the results presented in the main text (Fig S14).

4. Examination of posterior estimates for all model parameters

To diagnose posterior estimates for each parameter, we plotted the posterior median, 50% and 95% credible intervals (CrIs) estimated for each week during the entire study period, for each of the nine provinces (Figs. S15 – S23). As shown in Fig S15, the estimated transmission rate was relatively stable during the ancestral wave; it then increased along with the surge of the Beta variant around October 2020 and leveled off during the Beta wave. Similarly, following the initial surge of the Delta and Omicron variants, estimated transmission rates increased before leveling off when the new variant became predominant. Similar patterns are estimated for all provinces, indicating the model-inference system is able to capture the changes in transmission rate due to each new variant.

Estimated latent period (Fig S16), infectious period (Fig S17), immunity period (Fig S18), and the scaling factor of NPI effectiveness (Fig S19) all varied somewhat over time, but to a much less extent compared to the transmission rate. Estimated time from infectiousness to case detection decreased slightly over time, albeit with larger variations in later time periods (see Fig S20 for the mean and Fig S21 for the standard deviation). It is possible that the model-inference system could not adequately estimate the nuanced changes in these parameters using aggregated population level data.

Estimated infection-detection rates varied over time for all provinces (Fig S22). The infection-detection rate can be affected by 1) testing capacity, e.g., lower during the first weeks of the COVID-19 pandemic, and sometimes lower near the peak of a pandemic wave when maximal

capacity was reached; 2) awareness of the virus, e.g., higher when a new variant was first reported and lower near the end of a wave; and 3) disease severity, e.g., higher when variants causing more severe disease were circulating. Overall, the estimates were consistent with these expected patterns.

Lastly, estimated IFRs also varied over time and across provinces (Fig S23). IFR can be affected by multiple factors, including infection demographics, innate severity of the circulating variant, quality and access to healthcare, and vaccination coverage. For infection demographics, IFR tended to be much lower in younger ages as reported by many (e.g., Levin et al. 2020 *(5)*). In South Africa, similar differences in infection demographics occurred across provinces. For instance, Giandhari et al. (6) noted a lower initial mortality in Gauteng, as earlier infections concentrated in younger and wealthier individuals. For the innate severity of the circulating variant, as noted in the main text, in general estimated IFRs were higher during the Beta and Delta waves than during the Omicron wave. In addition, as shown in Fig S23, estimated IFRs were substantially higher in four provinces (i.e., KwaZulu-Natal, Western Cape, Eastern Cape, and Free State) than other provinces during the Beta wave. Coincidentally, the earliest surges of the Beta variant occurred in three of those provinces (i.e., KwaZulu-Natal, Western Cape, Eastern Cape)(7). Nonetheless, and as noted in the main text and the above subsection, the IFR estimates here should be interpreted with caution, due to the likely underreporting and irregularity of the COVID-19 mortality data used to generate these estimates.

5. A proposed approach to compute the reinfection rates using model-inference estimates.
It is difficult to measure or estimate reinfection rate directly. In this study, we have estimated the immune erosion potential for three major SARS-CoV-2 variants of concern (VOCs) and the infection rates during each pandemic wave in South Africa. These estimates can be used to support estimation of the reinfection rate for a given population. In-depth analysis is needed for such estimations. Here, as an example, we propose a simple approach to illustrate the possibility.

Consider the estimation in the context of the four waves in South Africa in this study (i.e., ancestral, Beta, Delta, and Omicron BA.1 wave). Suppose the cumulative fraction of the population *ever infected before the beta wave is* c_{pre_beta} *(this is roughly the attack rate during the ancestral wave)* and estimated immune erosion potential for Beta is θ_{beta}. To compute the reinfection rate during the Beta wave, we can assume that $c_{pre\_beta} \times (1 - \theta_{beta})$ are protected by this prior immunity, and that the remaining $c_{pre\_beta}\theta_{beta}$ (i.e. those lost their immunity due to immune erosion) have the same risk of infection as those never infected, such that the reinfection rate/fraction *among all infections,* z_{beta}, during the Beta wave (i.e., z_{beta} is the attack rate by Beta) would be:

$$\eta_{beta} = \frac{c_{pre\_beta}\theta_{beta}}{1 - c_{pre\_beta} + c_{pre\_beta}\theta_{beta}}$$

The reinfection rate/fraction among the entire population would be:

$$\eta'_{beta} = z_{beta}\eta_{beta}$$

Combining the above, the cumulative fraction of the population *ever infected by the end of the Beta wave* and *before the Delta wave* would be:

$$c_{pre\_delta} = c_{pre\_beta} + z_{beta} - \eta'_{beta}$$

Note that the fraction of the population *ever infected*, *c*, is updated to compute the subsequent fraction of the population protected by prior immunity, because the immune erosion potential here is estimated relative to the combined immunity accumulated until the rise of a new variant. We can repeat the above process for the Delta wave and the Omicron wave. See an example calculation in Table S4.

Work to refine the reinfection estimates (e.g., sensitivity of these estimates to assumptions and uncertainty intervals) is needed. Nonetheless, these example estimates (Table S4) are consistent with reported serology measures [4th column vs. e.g. ~90% seropositive in March 2022 after the Omicron BA.1 wave reported in Bingham et al. 2022 (8)] and reinfection rates reported elsewhere [5th and 6th columns vs. e.g., reported much higher reinfection rate during the Omicron wave in Pulliam et al. (9)]. Importantly, these estimates also show that, in addition to the innate immune erosive potential of a given new variant, the reinfection rate is also determined by the prior cumulative fraction of the population ever infected (4th column in Table S4) and the attack rate by each variant (3rd column in Table S4). That is, the higher the prior cumulative infection rate and/or the higher the attack rate by the new variant, the higher the reinfection rate would be for a new variant that can cause reinfection. For instance, despite the lower immune erosion potential of Delta than Beta, because of the high prior infection rate accumulated up to the Delta wave onset, the estimated reinfection rate by Delta *among all Delta infections* was higher compared to that during the Beta wave (6th column in Table S4). With the higher attack rate during the Delta wave, the reinfection rate *among the entire population* was much higher for Delta than Beta (5th column in Table S4). Thus, these preliminary results suggest that reinfection rates observed for each variant and differences across different variants should be interpreted in the context of the innate immune erosion potential of each variant, the prior cumulative infection rate of the study population, and the attack rate of each variant in the same population.

Reference:

1. FT Visual & Data Journalism team (Coronavirus tracked: see how your country compares.
2. Anderson JL (2001) An ensemble adjustment Kalman filter for data assimilation. *Mon. Weather Rev.* 129(12):2884-2903.
3. Yang W & Shaman J (2014) A simple modification for improving inference of non-linear dynamical systems. *arXiv*:1403.6804.
4. Yang W & Shaman J (2021) Development of a model-inference system for estimating epidemiological characteristics of SARS-CoV-2 variants of concern. *Nature Communications* 12:5573.
5. Levin AT*, et al.* (2020) Assessing the age specificity of infection fatality rates for COVID-19: systematic review, meta-analysis, and public policy implications. *Eur J Epidemiol* 35(12):1123-1138.
6. Giandhari J*, et al.* (2021) Early transmission of SARS-CoV-2 in South Africa: An epidemiological and phylogenetic report. *Int J Infect Dis* 103:234-241.
7. Tegally H*, et al.* (2021) Detection of a SARS-CoV-2 variant of concern in South Africa. *Nature* 592(7854):438-443.
8. Bingham J*, et al.* (2022) Estimates of prevalence of anti-SARS-CoV-2 antibodies among blood donors in South Africa in March 2022.
9. Pulliam JRC*, et al.* (2022) Increased risk of SARS-CoV-2 reinfection associated with emergence of Omicron in South Africa. *Science* 376(6593):eabn4947.

Supplemental Figures and Tables

Fig S1. Model-fit to case and death data in each province. Dots show reported SARS-CoV-2 cases and deaths by week. Blue lines and surrounding area show model estimated median, 50% (darker blue) and 95% (lighter blue) credible intervals. Note that reported mortality was high in February 2022 in some provinces with no clear explanation.

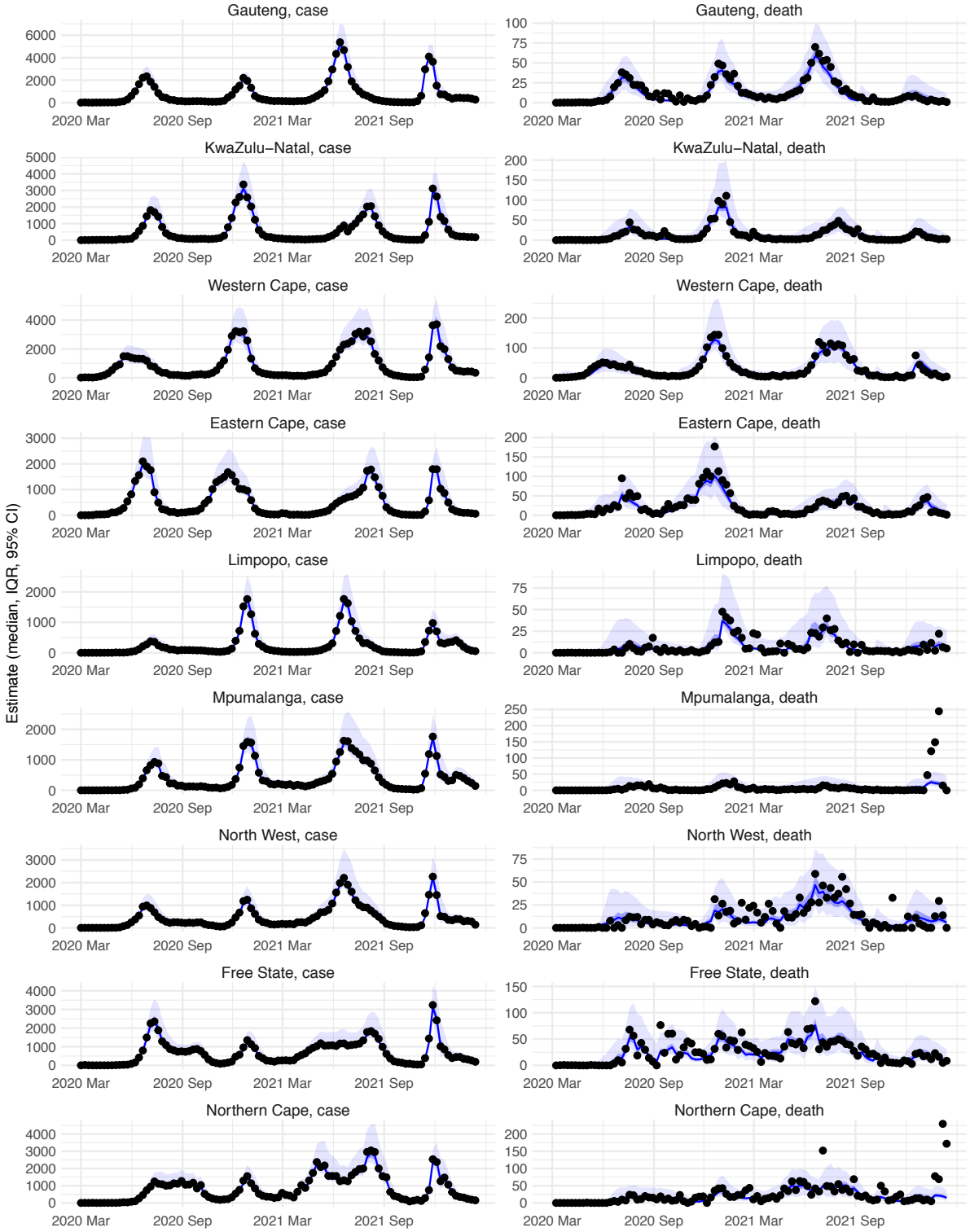

Fig S2. Model validation using hospitalization and excess mortality data. Model estimated infection rates are compared to COVID-related hospitalizations (left panel) and excess mortality (right panel) during the Ancestral (A), Beta (B), Delta (C), and Omicron (D) waves. Boxplots show the estimated distribution for each province (middle bar = mean; edges = 50% CrIs and whiskers =95% CrIs). Red dots show COVID-related hospitalizations (left panel, right y-axis) and excess mortality (right panel, right y-axis); these are independent measurements *not* used for model fitting. Correlation (*r*) is computed between model estimates (i.e., median cumulative infection rates for the nine provinces) and the independent measurements (i.e., hospitalizations in the nine provinces in left panel, and age-adjusted excess mortality in the right panel), for each wave. *Note that hospitalization data begin from 6/6/20 and excess mortality data begin from 5/3/20 and thus are incomplete for the ancestral wave.*

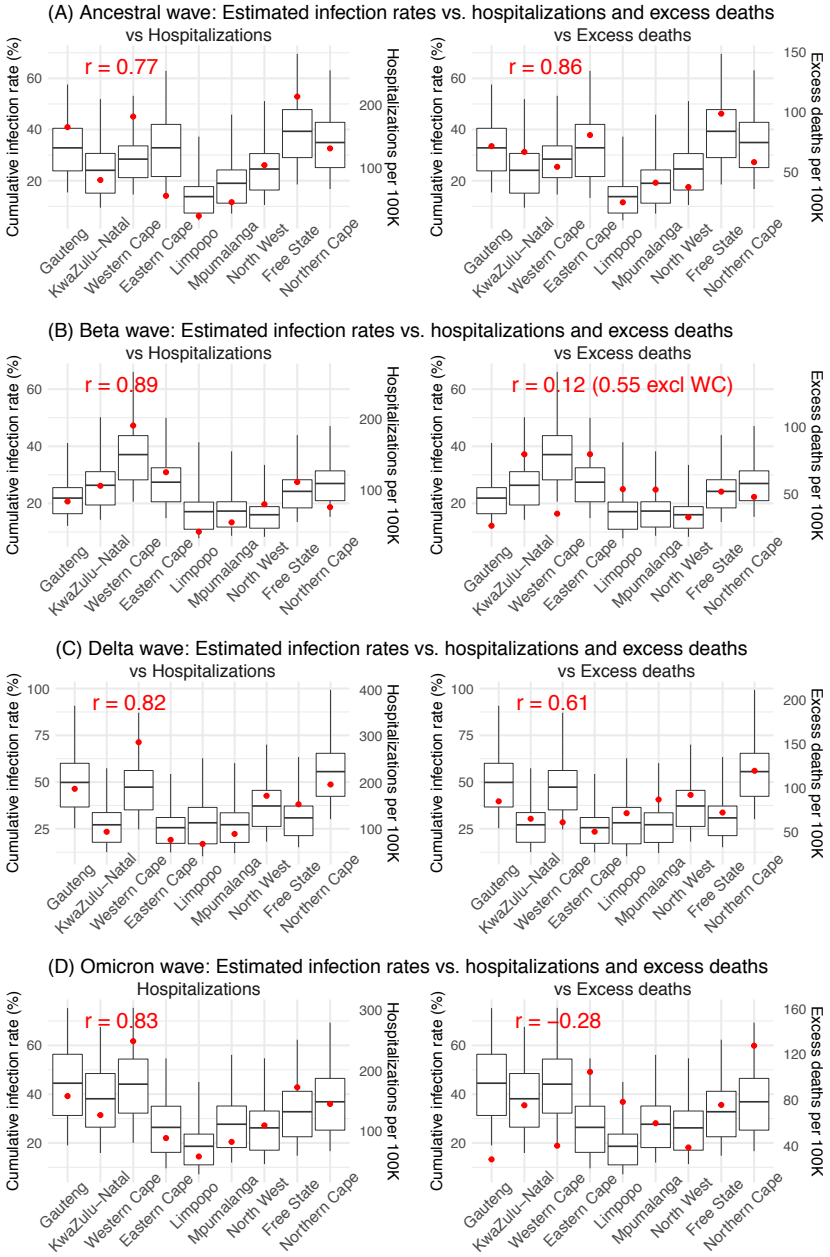

Fig S3. Model validation using retrospective prediction, for the remaining 5 provinces. Model-inference was trained on cases and deaths data since March 15, 2020 until 2 weeks (1st plot in each panel) or 1 week (2nd plot) before the Delta or Omicron wave (see timing on the x-axis); the model was then integrated forward using the estimates made at the time to predict cases (left panel) and deaths (right panel) for the remaining weeks of each wave. Blue lines and surrounding shades show model fitted cases and deaths for weeks before the prediction (line = median, dark blue area = 50% CrIs, and light blue = 80% CrIs). Red lines show model projected median weekly cases and deaths; surrounding shades show 50% (dark red) and 80% (light red) CIs of the prediction. For comparison, reported cases and deaths for each week are shown by the black dots; however, those to the right of the vertical dash lines (showing the start of each prediction) were not used in the model. For clarity, here we show 80% CIs (instead of 95% CIs, which tend to be wider for longer-term projections) and predictions for the five least populous provinces (Limpopo in A and B; Mpumalanga in C and D; North West in E and F; Free State in G and H; and Northern Cape in I and J). Predictions for the other 4 provinces are shown in Fig 2.

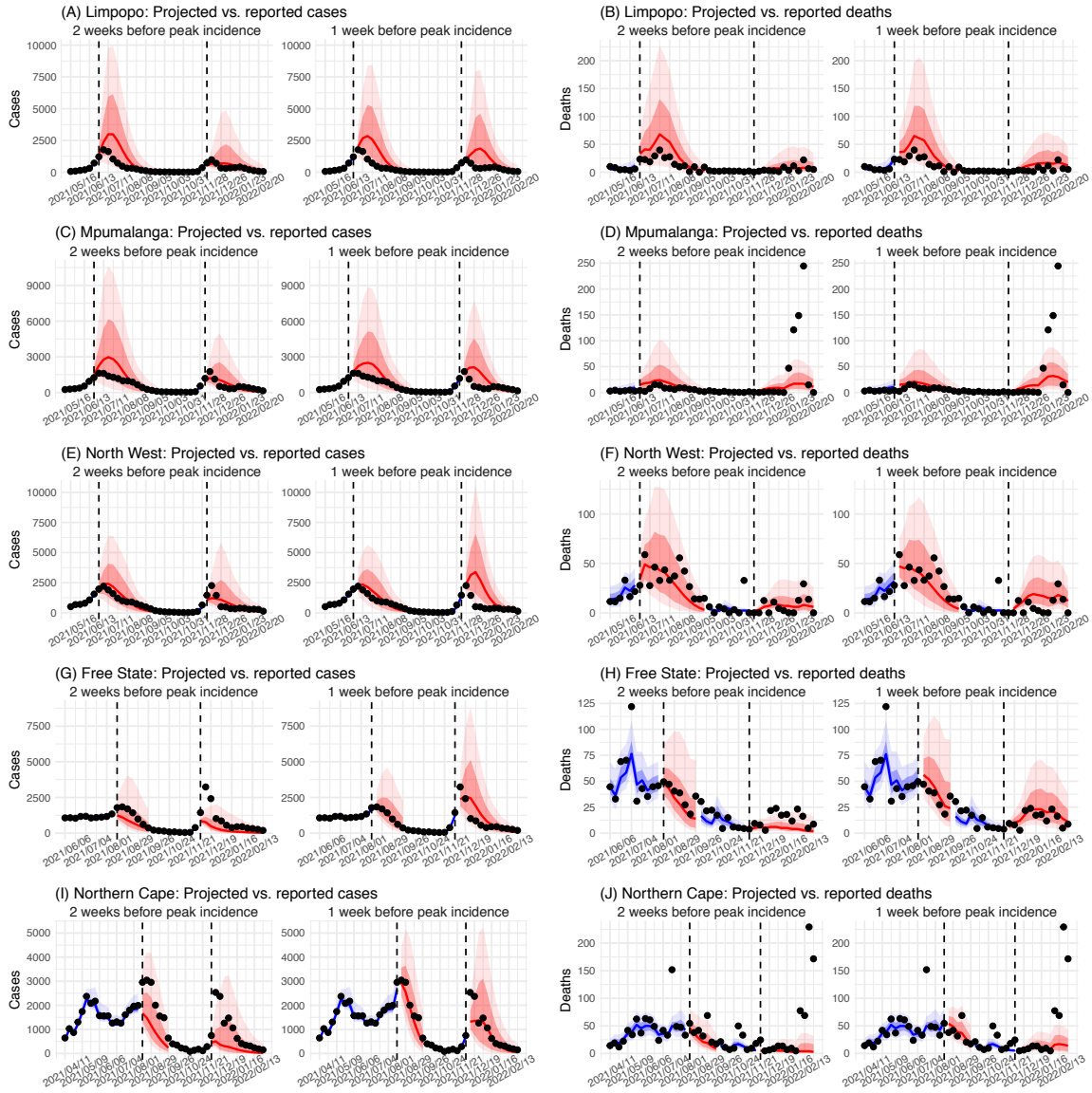

Fig S4. Model inference estimates for *KwaZulu-Natal*. (A) Observed relative mobility, vaccination rate, and estimated disease seasonal trend, compared to case and death rates over time. Key model-inference estimates are shown for the time-varying effective reproduction number R_t (B), transmissibility R_{TX} (C), population susceptibility (D, shown relative to the population size in percentage), infection-detection rate (E), and infection-fatality risk (F). Grey shaded areas indicate the approximate circulation period for each variant. In (B) – (F), blue lines and surrounding areas show the estimated mean, 50% (dark) and 95% (light) CrIs; boxes and whiskers show the estimated mean, 50% and 95% CrIs for estimated infection rates. *Note that the transmissibility estimates (R_{TX} in C) have removed the effects of changing population susceptibility, NPIs, and disease seasonality; thus, the trends are more stable than the reproduction number (R_t in B) and reflect changes in variant-specific properties. Also note that infection-fatality risk estimates were based on reported COVID-19 deaths and may not reflect true values due to likely under-reporting of COVID-19 deaths.*

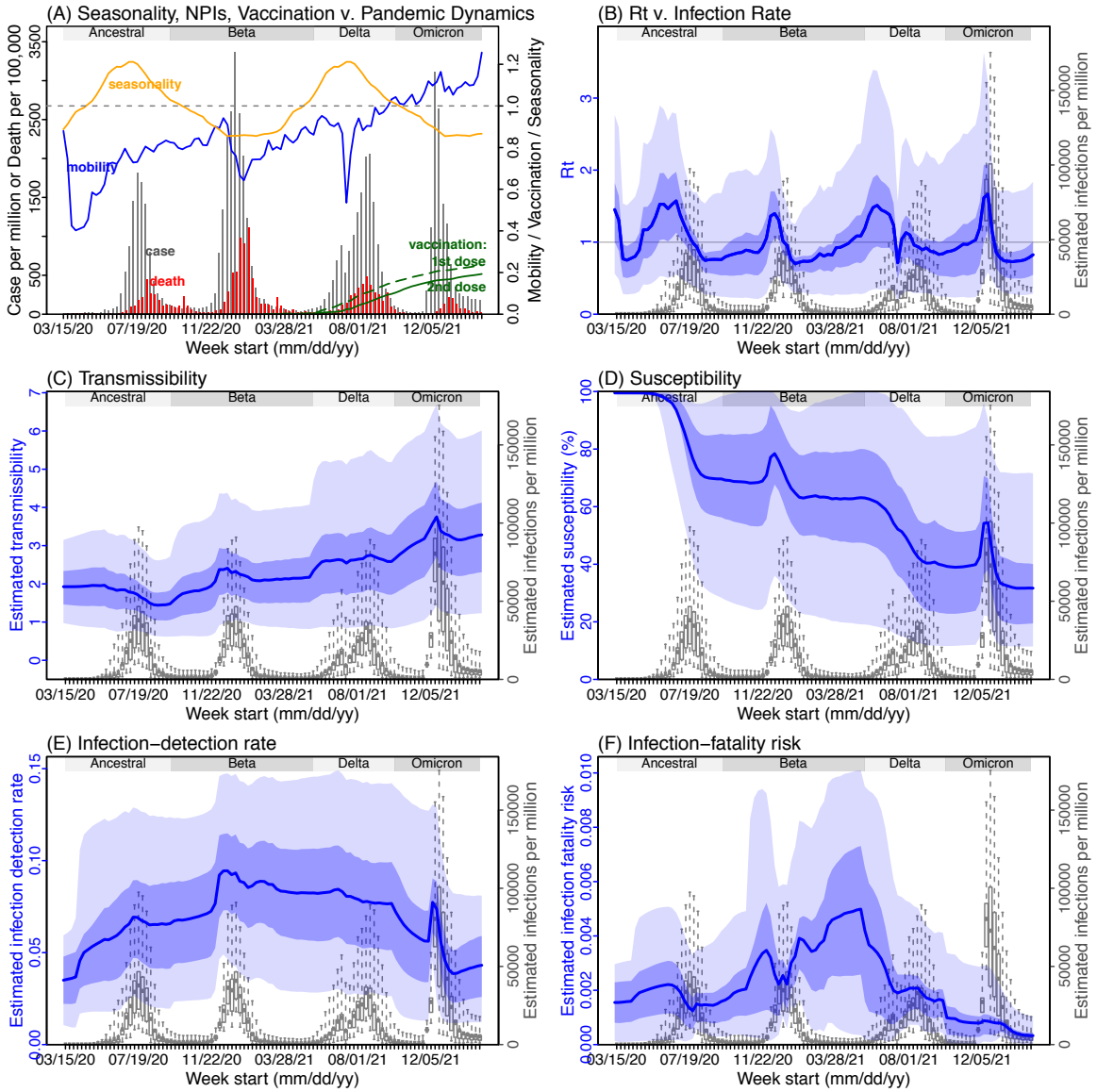

Fig S5. Model inference estimates for *Western Cape*. (A) Observed relative mobility, vaccination rate, and estimated disease seasonal trend, compared to case and death rates over time. Key model-inference estimates are shown for the time-varying effective reproduction number R_t (B), transmissibility R_{TX} (C), population susceptibility (D, shown relative to the population size in percentage), infection-detection rate (E), and infection-fatality risk (F). Grey shaded areas indicate the approximate circulation period for each variant. In (B) – (F), blue lines and surrounding areas show the estimated mean, 50% (dark) and 95% (light) CrIs; boxes and whiskers show the estimated mean, 50% and 95% CrIs for estimated infection rates. *Note that the transmissibility estimates (R_{TX} in C) have removed the effects of changing population susceptibility, NPIs, and disease seasonality; thus, the trends are more stable than the reproduction number (R_t in B) and reflect changes in variant-specific properties. Also note that infection-fatality risk estimates were based on reported COVID-19 deaths and may not reflect true values due to likely under-reporting of COVID-19 deaths.*

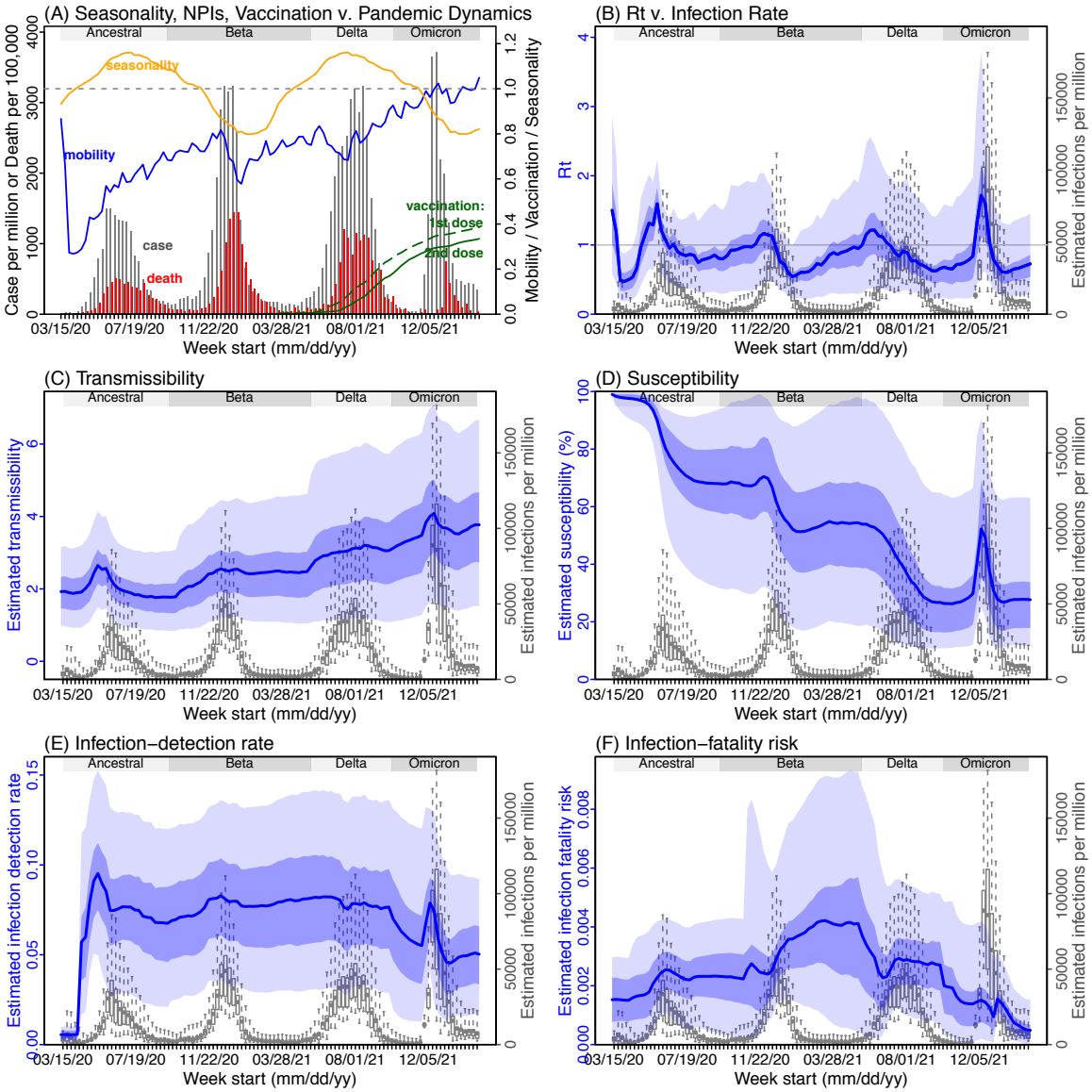

Fig S6. Model inference estimates for *Eastern Cape*. (A) Observed relative mobility, vaccination rate, and estimated disease seasonal trend, compared to case and death rates over time. Key model-inference estimates are shown for the time-varying effective reproduction number R_t (B), transmissibility R_{TX} (C), population susceptibility (D, shown relative to the population size in percentage), infection-detection rate (E), and infection-fatality risk (F). Grey shaded areas indicate the approximate circulation period for each variant. In (B) – (F), blue lines and surrounding areas show the estimated mean, 50% (dark) and 95% (light) CrIs; boxes and whiskers show the estimated mean, 50% and 95% CrIs for estimated infection rates. *Note that the transmissibility estimates (R_{TX} in C) have removed the effects of changing population susceptibility, NPIs, and disease seasonality; thus, the trends are more stable than the reproduction number (R_t in B) and reflect changes in variant-specific properties. Also note that infection-fatality risk estimates were based on reported COVID-19 deaths and may not reflect true values due to likely under-reporting of COVID-19 deaths.*

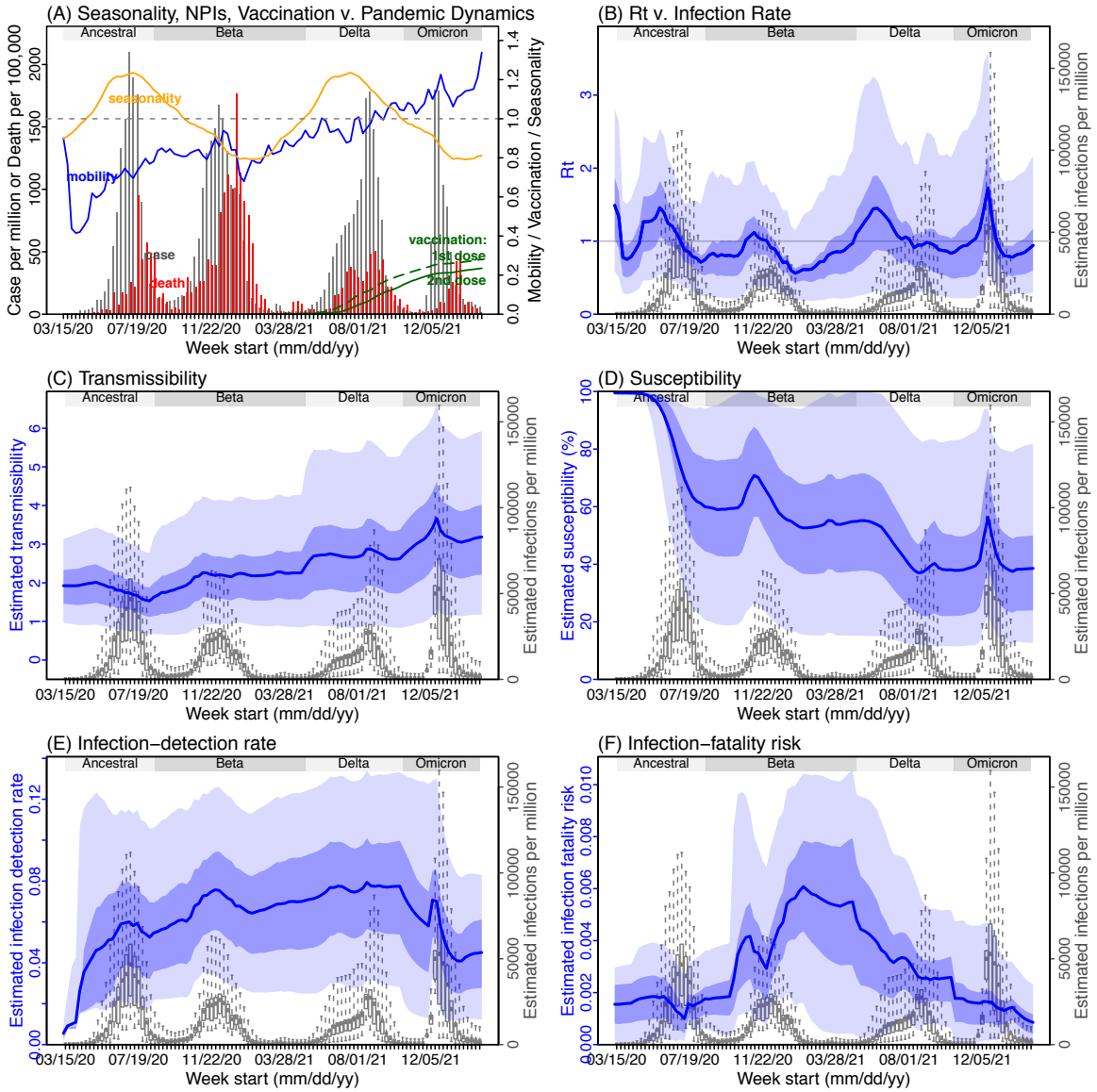

Fig S7. Model inference estimates for *Limpopo*. (A) Observed relative mobility, vaccination rate, and estimated disease seasonal trend, compared to case and death rates over time. Key model-inference estimates are shown for the time-varying effective reproduction number R_t (B), transmissibility R_{TX} (C), population susceptibility (D, shown relative to the population size in percentage), infection-detection rate (E), and infection-fatality risk (F). Grey shaded areas indicate the approximate circulation period for each variant. In (B) – (F), blue lines and surrounding areas show the estimated mean, 50% (dark) and 95% (light) CrIs; boxes and whiskers show the estimated mean, 50% and 95% CrIs for estimated infection rates. *Note that the transmissibility estimates (R_{TX} in C) have removed the effects of changing population susceptibility, NPIs, and disease seasonality; thus, the trends are more stable than the reproduction number (R_t in B) and reflect changes in variant-specific properties. Also note that infection-fatality risk estimates were based on reported COVID-19 deaths and may not reflect true values due to likely under-reporting of COVID-19 deaths.*

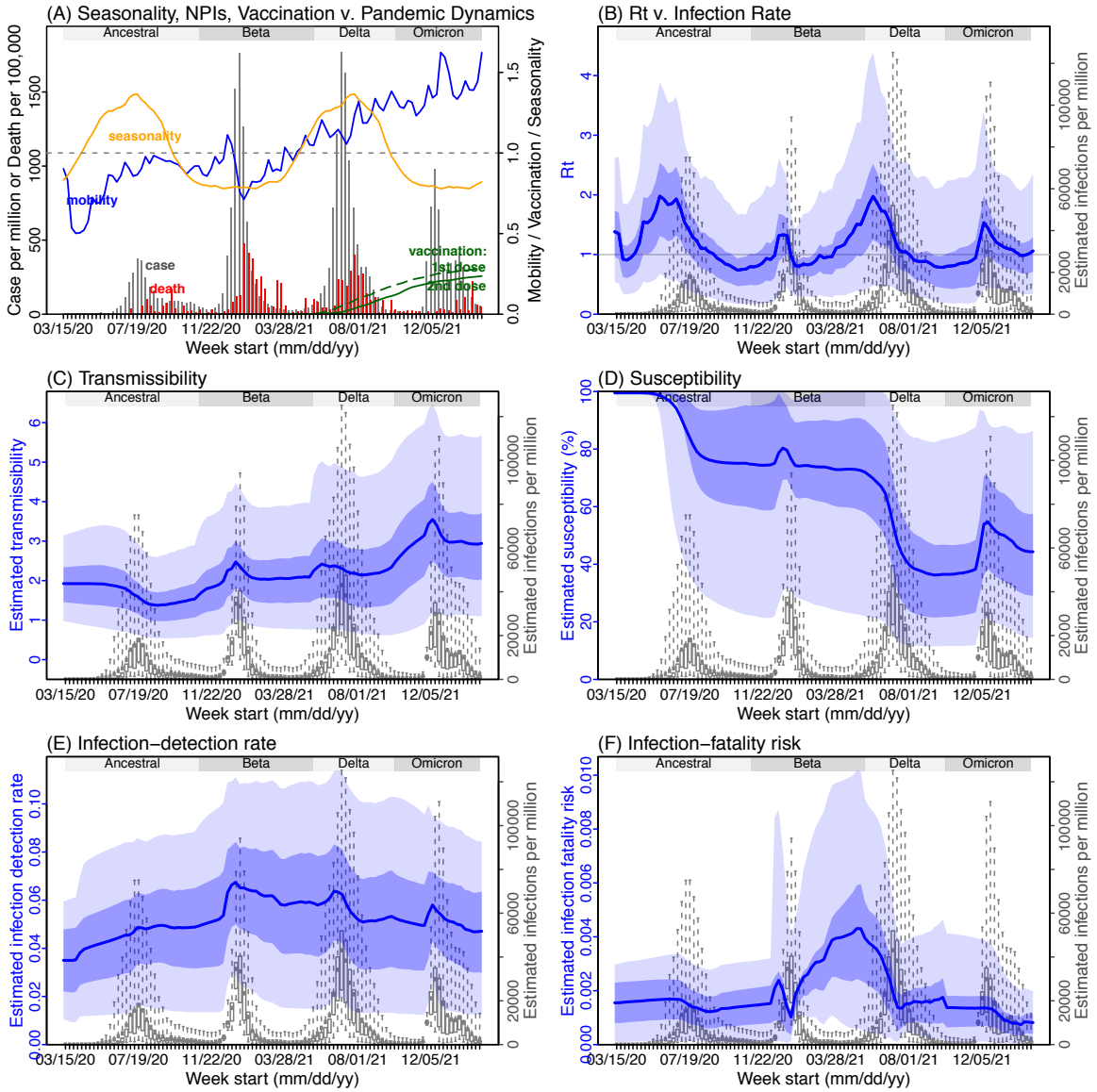

Fig S8. Model inference estimates for *Mpumalanga*. (A) Observed relative mobility, vaccination rate, and estimated disease seasonal trend, compared to case and death rates over time. Key model-inference estimates are shown for the time-varying effective reproduction number R_t (B), transmissibility R_{TX} (C), population susceptibility (D, shown relative to the population size in percentage), infection-detection rate (E), and infection-fatality risk (F). Grey shaded areas indicate the approximate circulation period for each variant. In (B) – (F), blue lines and surrounding areas show the estimated mean, 50% (dark) and 95% (light) CrIs; boxes and whiskers show the estimated mean, 50% and 95% CrIs for estimated infection rates. *Note that the transmissibility estimates (R_{TX} in C) have removed the effects of changing population susceptibility, NPIs, and disease seasonality; thus, the trends are more stable than the reproduction number (R_t in B) and reflect changes in variant-specific properties. Also note that infection-fatality risk estimates were based on reported COVID-19 deaths and may not reflect true values due to likely under-reporting of COVID-19 deaths.*

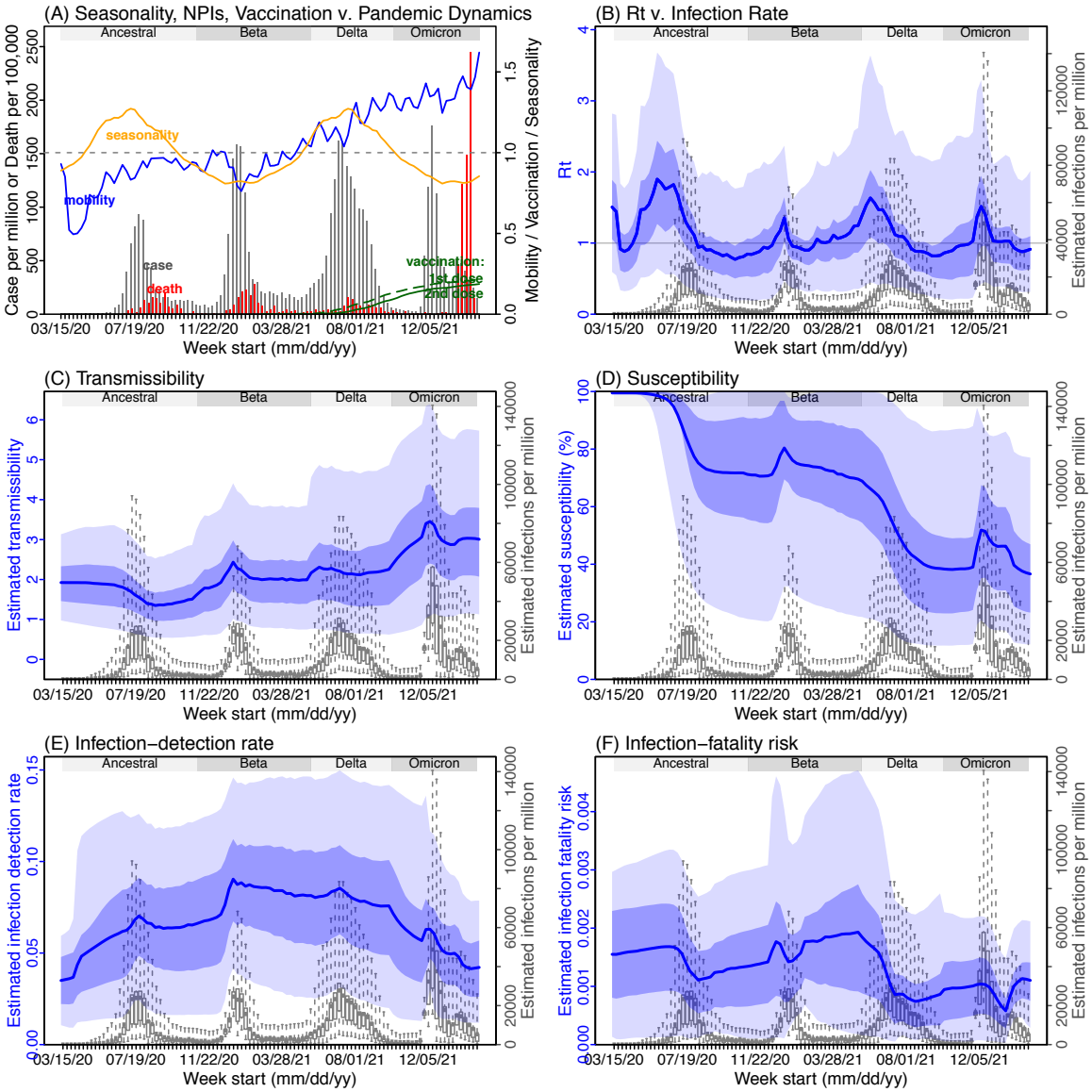

Fig S9. Model inference estimates for *North West*. (A) Observed relative mobility, vaccination rate, and estimated disease seasonal trend, compared to case and death rates over time. Key model-inference estimates are shown for the time-varying effective reproduction number R_t (B), transmissibility R_{TX} (C), population susceptibility (D, shown relative to the population size in percentage), infection-detection rate (E), and infection-fatality risk (F). Grey shaded areas indicate the approximate circulation period for each variant. In (B) – (F), blue lines and surrounding areas show the estimated mean, 50% (dark) and 95% (light) CrIs; boxes and whiskers show the estimated mean, 50% and 95% CrIs for estimated infection rates. *Note that the transmissibility estimates (R_{TX} in C) have removed the effects of changing population susceptibility, NPIs, and disease seasonality; thus, the trends are more stable than the reproduction number (R_t in B) and reflect changes in variant-specific properties. Also note that infection-fatality risk estimates were based on reported COVID-19 deaths and may not reflect true values due to likely under-reporting of COVID-19 deaths.*

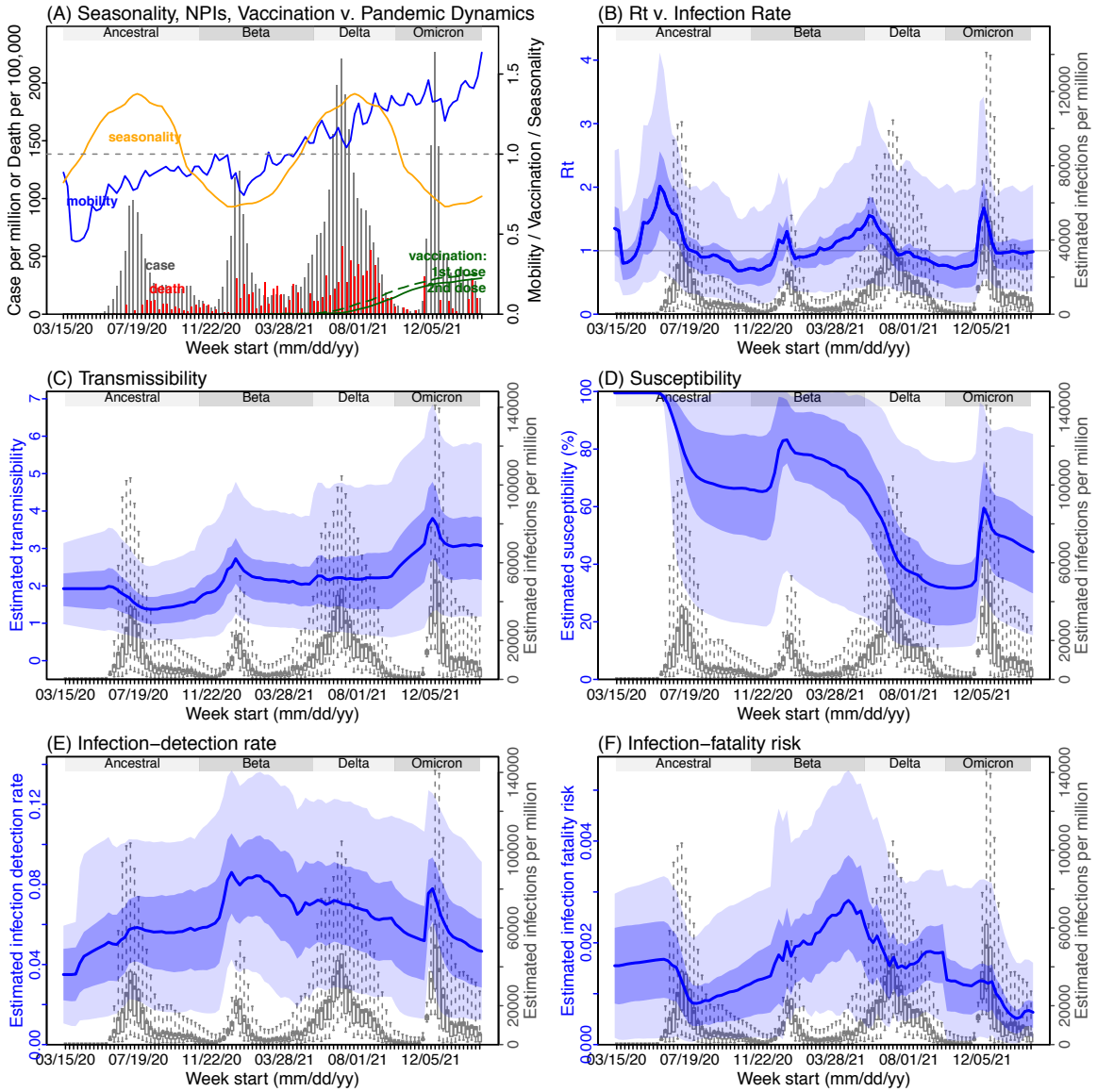

Fig S10. Model inference estimates for *Free State*. (A) Observed relative mobility, vaccination rate, and estimated disease seasonal trend, compared to case and death rates over time. Key model-inference estimates are shown for the time-varying effective reproduction number R_t (B), transmissibility R_{TX} (C), population susceptibility (D, shown relative to the population size in percentage), infection-detection rate (E), and infection-fatality risk (F). Grey shaded areas indicate the approximate circulation period for each variant. In (B) – (F), blue lines and surrounding areas show the estimated mean, 50% (dark) and 95% (light) CrIs; boxes and whiskers show the estimated mean, 50% and 95% CrIs for estimated infection rates. *Note that the transmissibility estimates (R_{TX} in C) have removed the effects of changing population susceptibility, NPIs, and disease seasonality; thus, the trends are more stable than the reproduction number (R_t in B) and reflect changes in variant-specific properties. Also note that infection-fatality risk estimates were based on reported COVID-19 deaths and may not reflect true values due to likely under-reporting of COVID-19 deaths.*

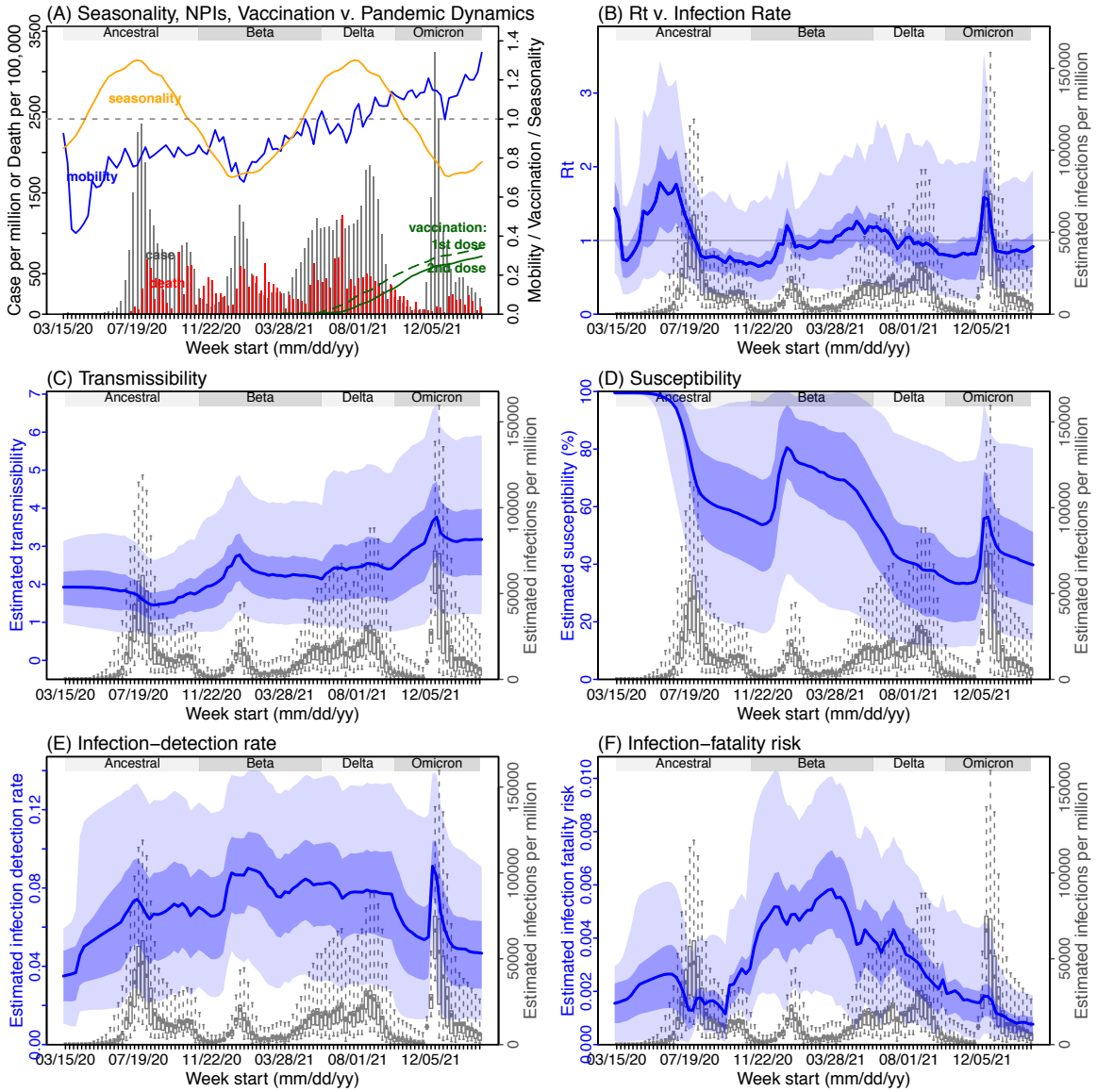

Fig S11. Model inference estimates for *Northern Cape*. (A) Observed relative mobility, vaccination rate, and estimated disease seasonal trend, compared to case and death rates over time. Key model-inference estimates are shown for the time-varying effective reproduction number R_t (B), transmissibility R_{TX} (C), population susceptibility (D, shown relative to the population size in percentage), infection-detection rate (E), and infection-fatality risk (F). Grey shaded areas indicate the approximate circulation period for each variant. In (B) – (F), blue lines and surrounding areas show the estimated mean, 50% (dark) and 95% (light) CrIs; boxes and whiskers show the estimated mean, 50% and 95% CrIs for estimated infection rates. *Note that the transmissibility estimates (R_{TX} in C) have removed the effects of changing population susceptibility, NPIs, and disease seasonality; thus, the trends are more stable than the reproduction number (R_t in B) and reflect changes in variant-specific properties. Also note that infection-fatality risk estimates were based on reported COVID-19 deaths and may not reflect true values due to likely under-reporting of COVID-19 deaths.*

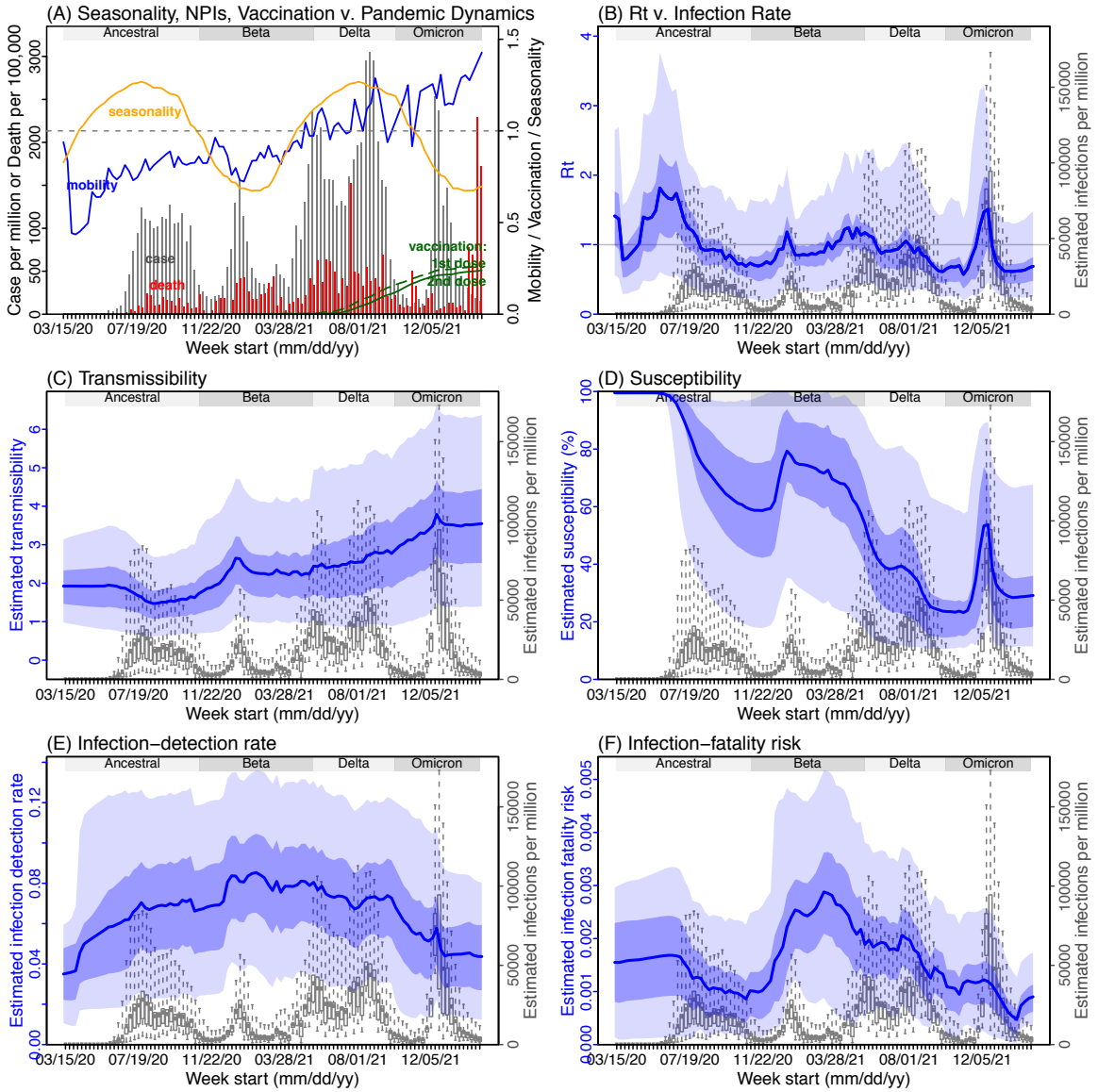

Fig S12. Comparison of posterior estimates for Gauteng during the Omicron (BA.1) wave, under four different settings for infection-detection rate. Four space reprobing (SR) settings for the infection-detection rate were tested and results are shown in the 4 four columns: 1) Use of the same baseline range as before (i.e., 1-8%) for all weeks during the Omicron (BA.1) wave; 2) Use of a wider and higher range (i.e., 1-12%) for all weeks; 3) Use of a range of 1-15% for the 1st week of Omicron detection, 5-20% for the 2nd week of Omicron detection, and 1-8% for the rest; and 4) Use of a range of 5-25% for the 2nd week of detection and 1-8% for all other weeks. Estimated infection-detection rates are shown in the 1st row, population susceptibility estimates are shown in the 2nd row, and transmissibility estimates are shown in the 3rd row. In each plot, blue lines and surrounding areas show the median, 50% and 95% CrIs of the posterior (left y-axis) for each week (x-axis). For comparison, reported cases for corresponding weeks are shown by the grey bars (right y-axis).

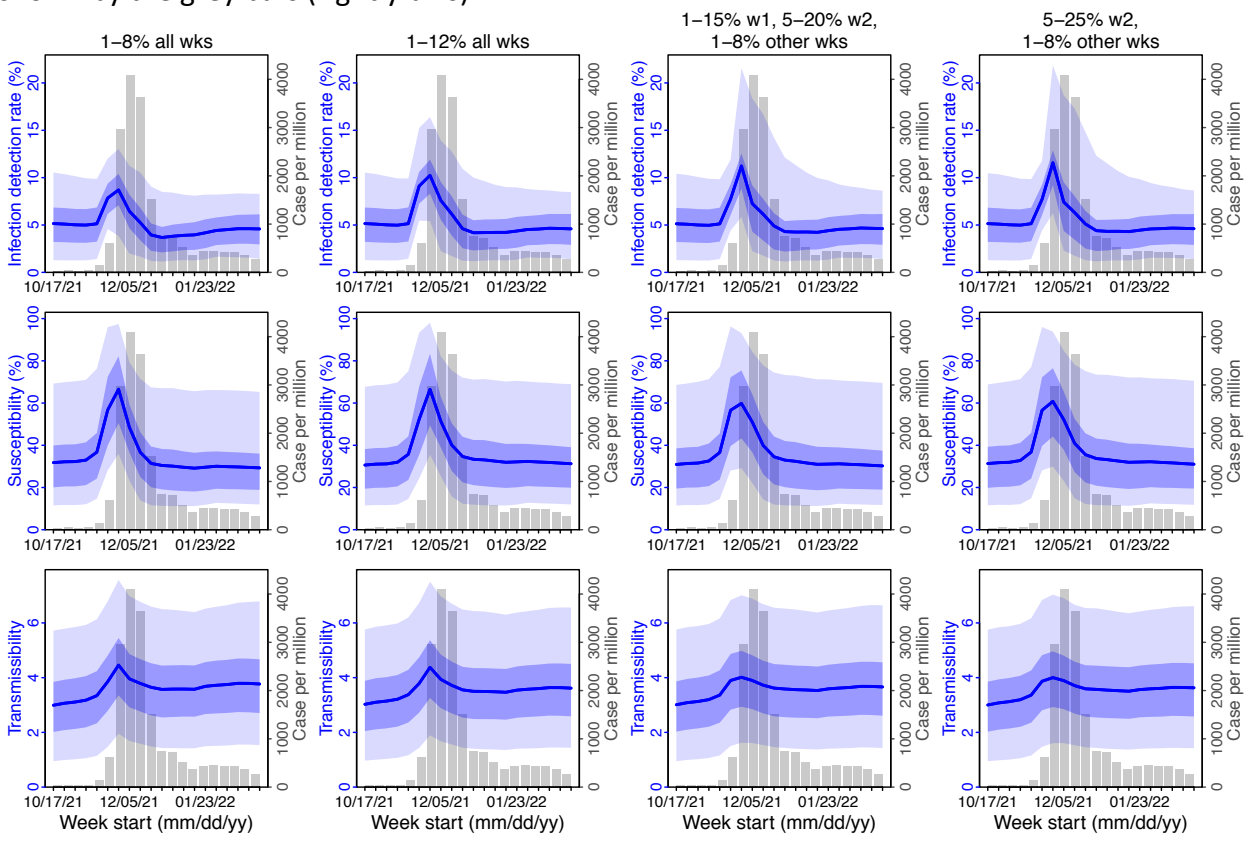

Fig S13. Comparison of retrospective prediction of the Omicron (BA.1) wave in Gauteng with the four different settings of infection-detection rate. Four space reprobing (SR) settings for the infection-detection rate were tested, and the results are shown in the 4 panels: 1) Use of the same baseline range as before (i.e., 1-8%) for all weeks during the Omicron (BA.1) wave; 2) Use of a wider and higher range (i.e., 1-12%) for all weeks; 3) Use of a range of 1-15% for the 1st week of Omicron detection, 5-20% for the 2nd week of Omicron detection, and 1-8% for the rest; and 4) Use of a range of 5-25% for the 2nd week of detection and 1-8% for all other weeks. Blue lines and show model fitted cases for weeks before the prediction. Red lines show model projected median weekly cases and deaths; surrounding shades show 50% (dark red) and 80% (light red) CIs of the prediction. For comparison, reported cases for each week are shown by the black dots; however, those to the right of the vertical dash lines (showing the start of each prediction) were not used in the model.

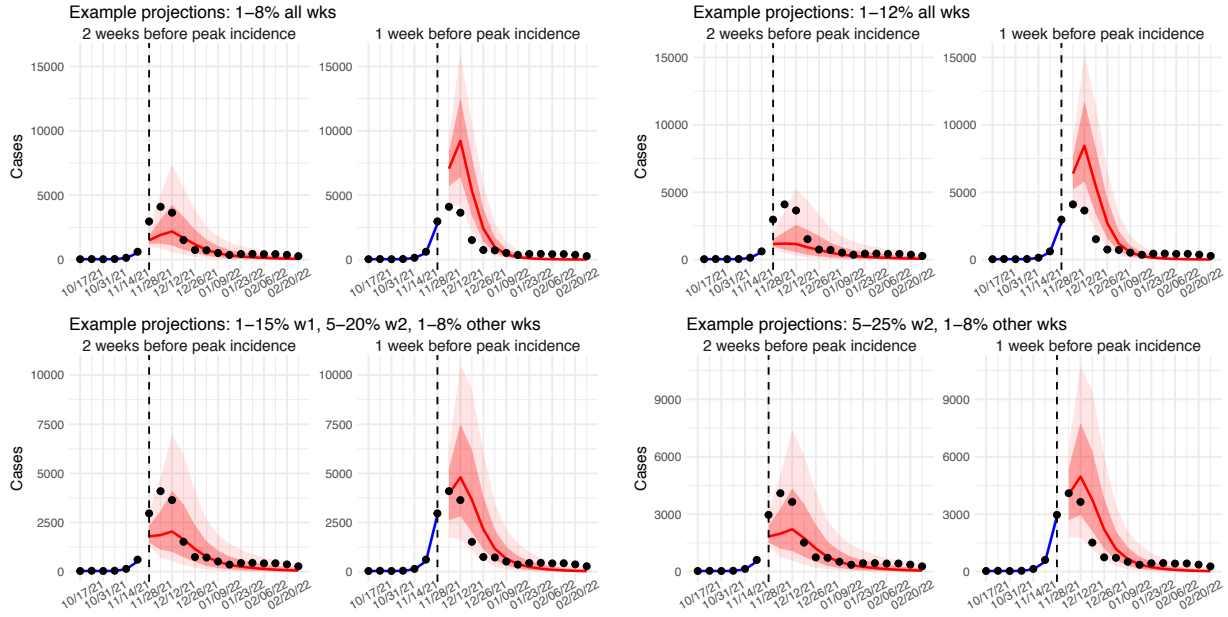

Fig S14. Comparison of the estimated increase in transmissibility and immune erosion for the Omicron (BA.1) variant in Gauteng, under four different settings of the infection-detection rate. Four space reprobing (SR) settings for the infection-detection rate were tested: 1) Use of the same baseline range as before (i.e., 1-8%) for all weeks during the Omicron (BA.1) wave; 2) Use of a wider and higher range (i.e., 1-12%) for all weeks; 3) Use of a range of 1-15% for the 1st week of Omicron detection, 5-20% for the 2nd week of Omicron detection, and 1-8% for the rest; and 4) Use of a range of 5-25% for the 2nd week of detection and 1-8% for all other weeks. Boxplots in left panel show the estimated distribution of increases in transmissibility, relative to the Ancestral SARS-CoV-2 (middle bar = median; edges = 50% CIs; and whiskers =95% CIs); boxplots in the right panel show the estimated distribution of immune erosion to all adaptive immunity gained from infection and vaccination prior to the surge of Omicron (BA.1) wave.

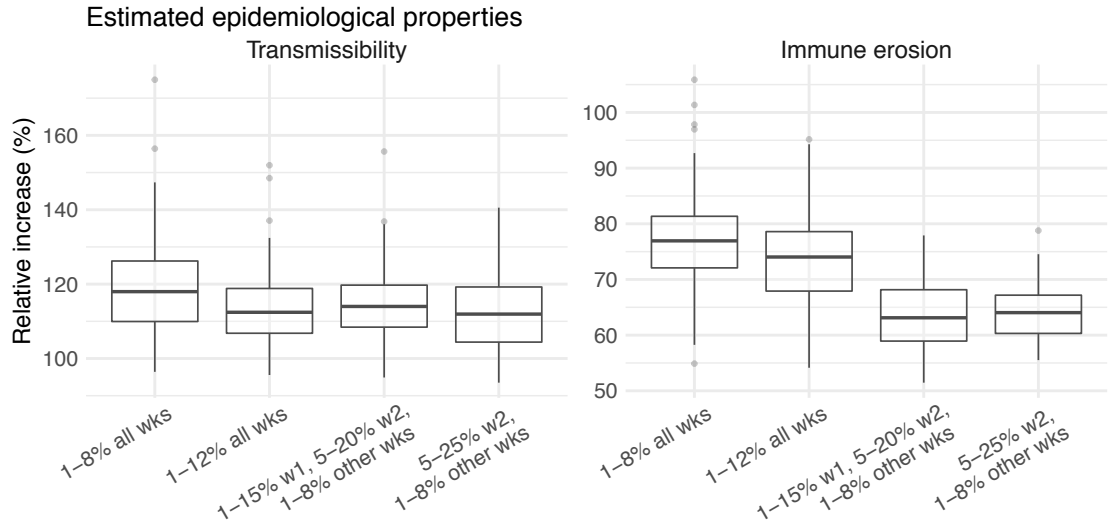

Fig S15. Posterior estimates for the transmission rate (β_t in Eqn 1) by week. Thick black lines show the median, dark blue areas show the 50% CrIs, and light blue areas show the 95% CrIs. For reference, the dashed vertical black lines indicate three dates (mm/dd/yy), i.e., 10/15/20, 5/15/21, and 11/15/21, roughly the start of the Beta, Delta, and Omicron waves, respectively.

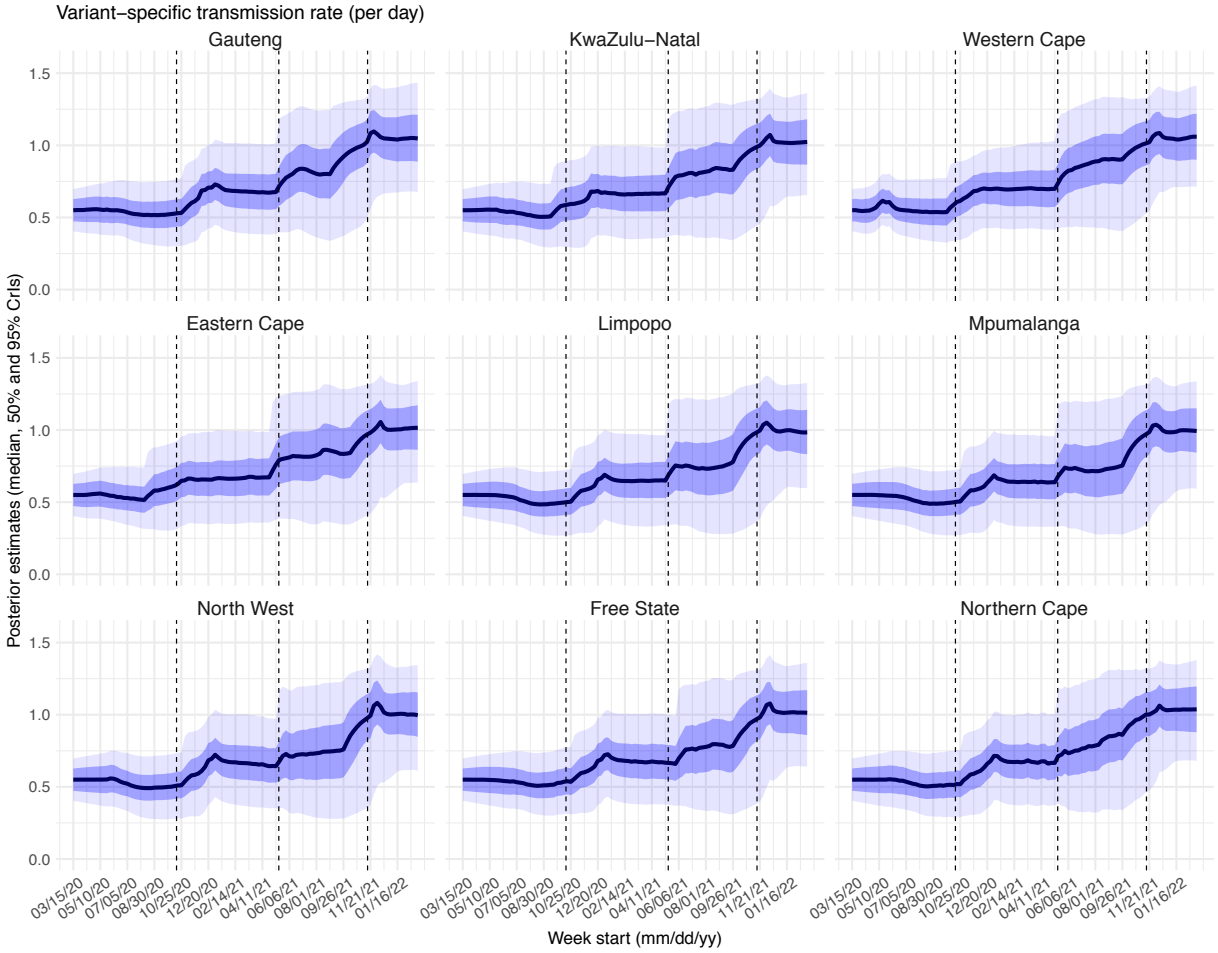

Fig S16. Posterior estimates for the latent period (Z_t in Eqn 1) by week. Thick black lines show the median, dark blue areas show the 50% CrIs, and light blue areas show the 95% CrIs. For reference, the dashed vertical black lines indicate three dates (mm/dd/yy), i.e., 10/15/20, 5/15/21, and 11/15/21, roughly the start of the Beta, Delta, and Omicron waves, respectively.

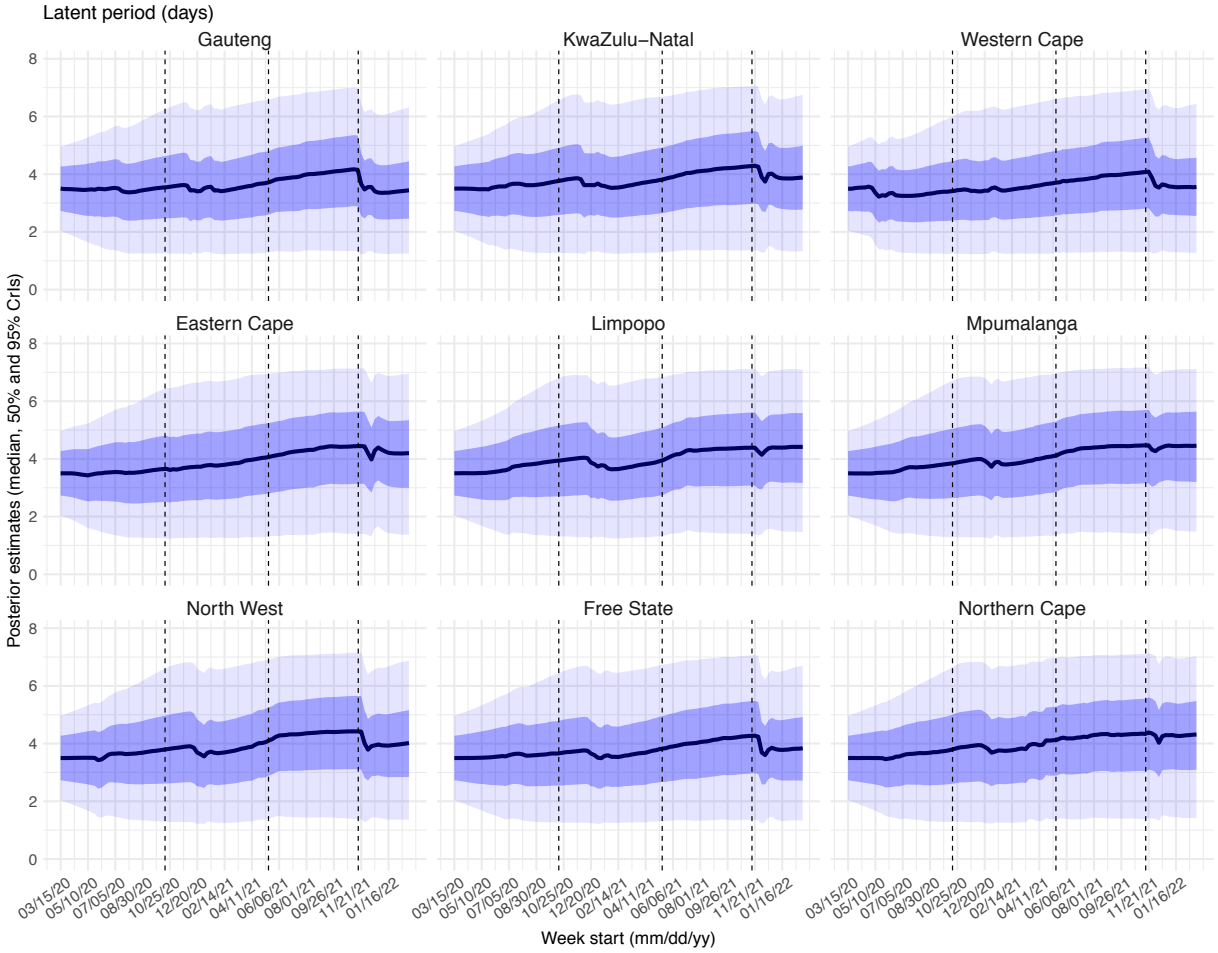

Fig S17. Posterior estimates for the infectious period (D_t in Eqn 1) by week. Thick black lines show the median, dark blue areas show the 50% CrIs, and light blue areas show the 95% CrIs. For reference, the dashed vertical black lines indicate three dates (mm/dd/yy), i.e., 10/15/20, 5/15/21, and 11/15/21, roughly the start of the Beta, Delta, and Omicron waves, respectively.

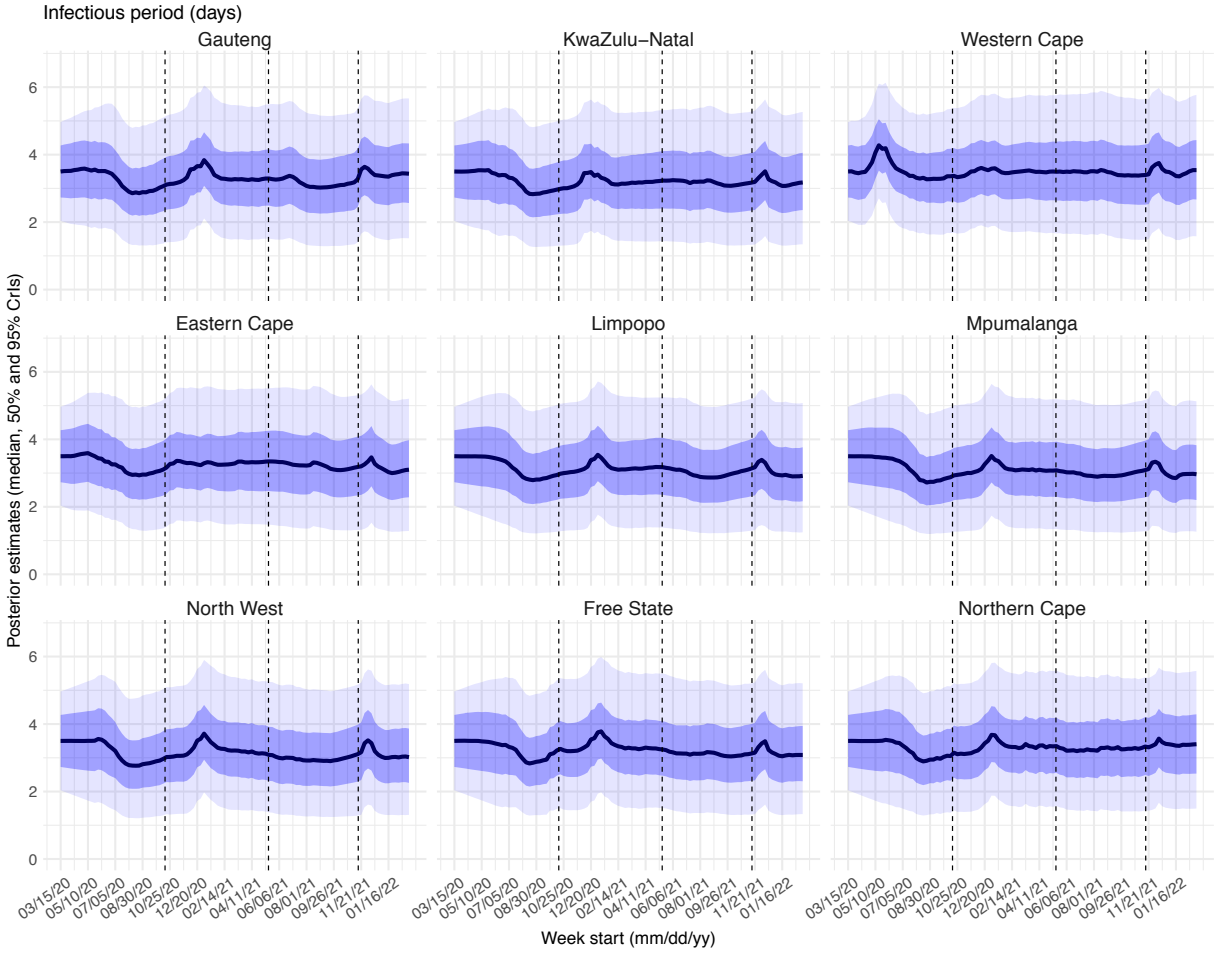

Fig S18. Posterior estimates for the immunity period (L_t in Eqn 1) by week. Thick black lines show the median, dark blue areas show the 50% CrIs, and light blue areas show the 95% CrIs. For reference, the dashed vertical black lines indicate three dates (mm/dd/yy), i.e., 10/15/20, 5/15/21, and 11/15/21, roughly the start of the Beta, Delta, and Omicron waves, respectively.

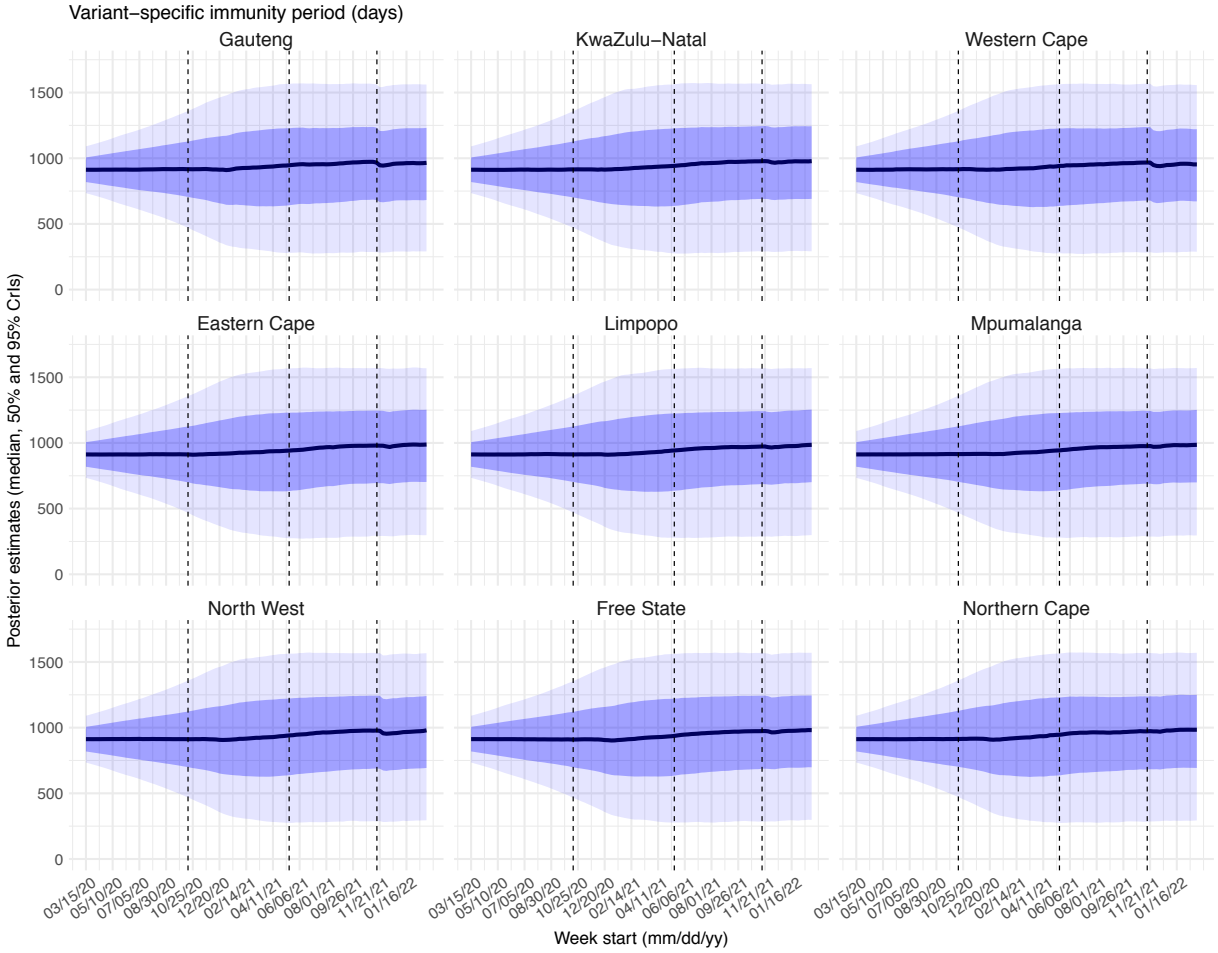

Fig S19. Posterior estimates for the scaling factor of NPI effectiveness (e_t in Eqn 1) by week. Thick black lines show the median, dark blue areas show the 50% CrIs, and light blue areas show the 95% CrIs. For reference, the dashed vertical black lines indicate three dates (mm/dd/yy), i.e., 10/15/20, 5/15/21, and 11/15/21, roughly the start of the Beta, Delta, and Omicron waves, respectively.

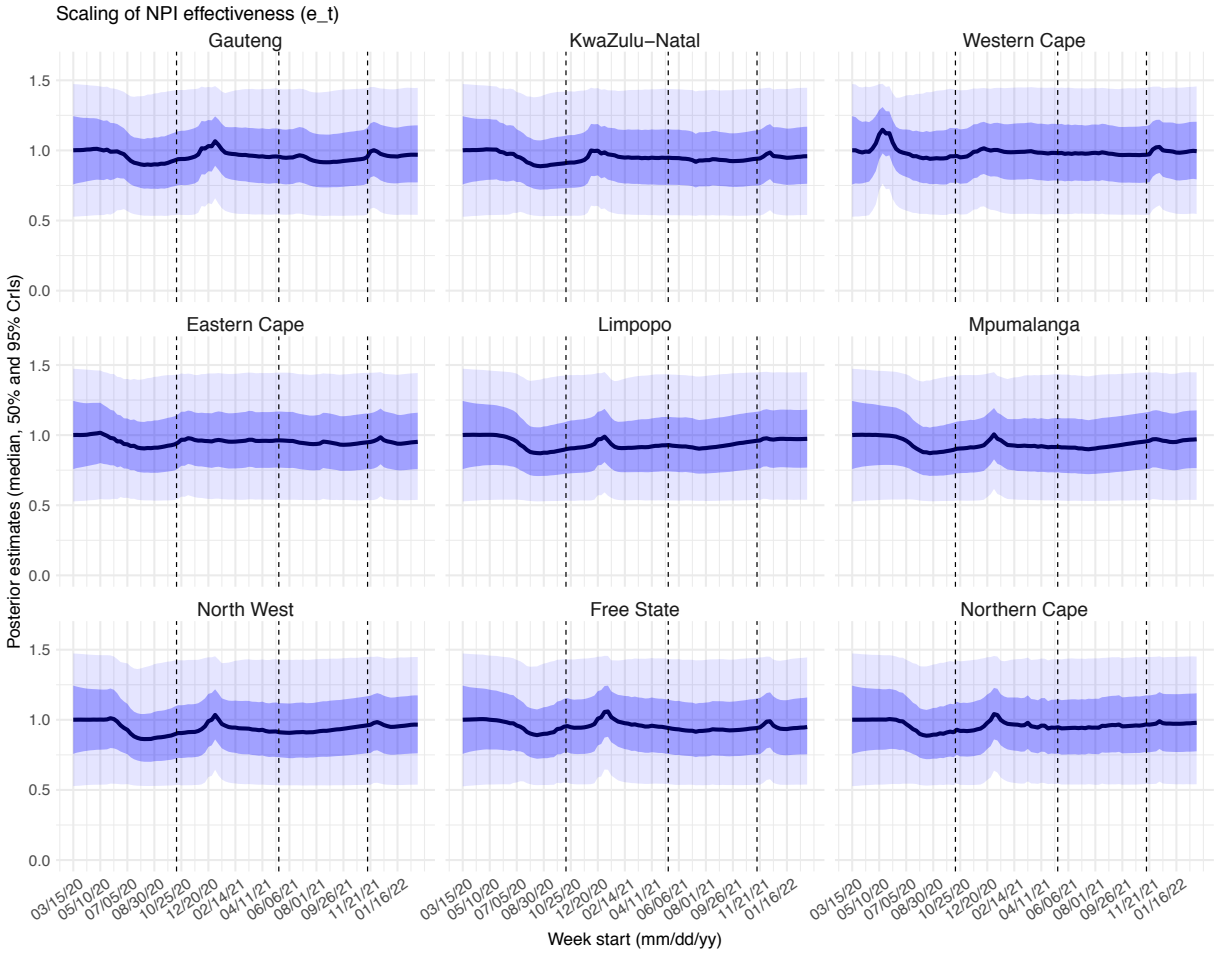

Fig S20. Posterior estimates for the mean of time from infectiousness to detection ($T_{d,mean}$ in the observation model) by week. Thick black lines show the median, dark blue areas show the 50% CrIs, and light blue areas show the 95% CrIs. For reference, the dashed vertical black lines indicate three dates (mm/dd/yy), i.e., 10/15/20, 5/15/21, and 11/15/21, roughly the start of the Beta, Delta, and Omicron waves, respectively.

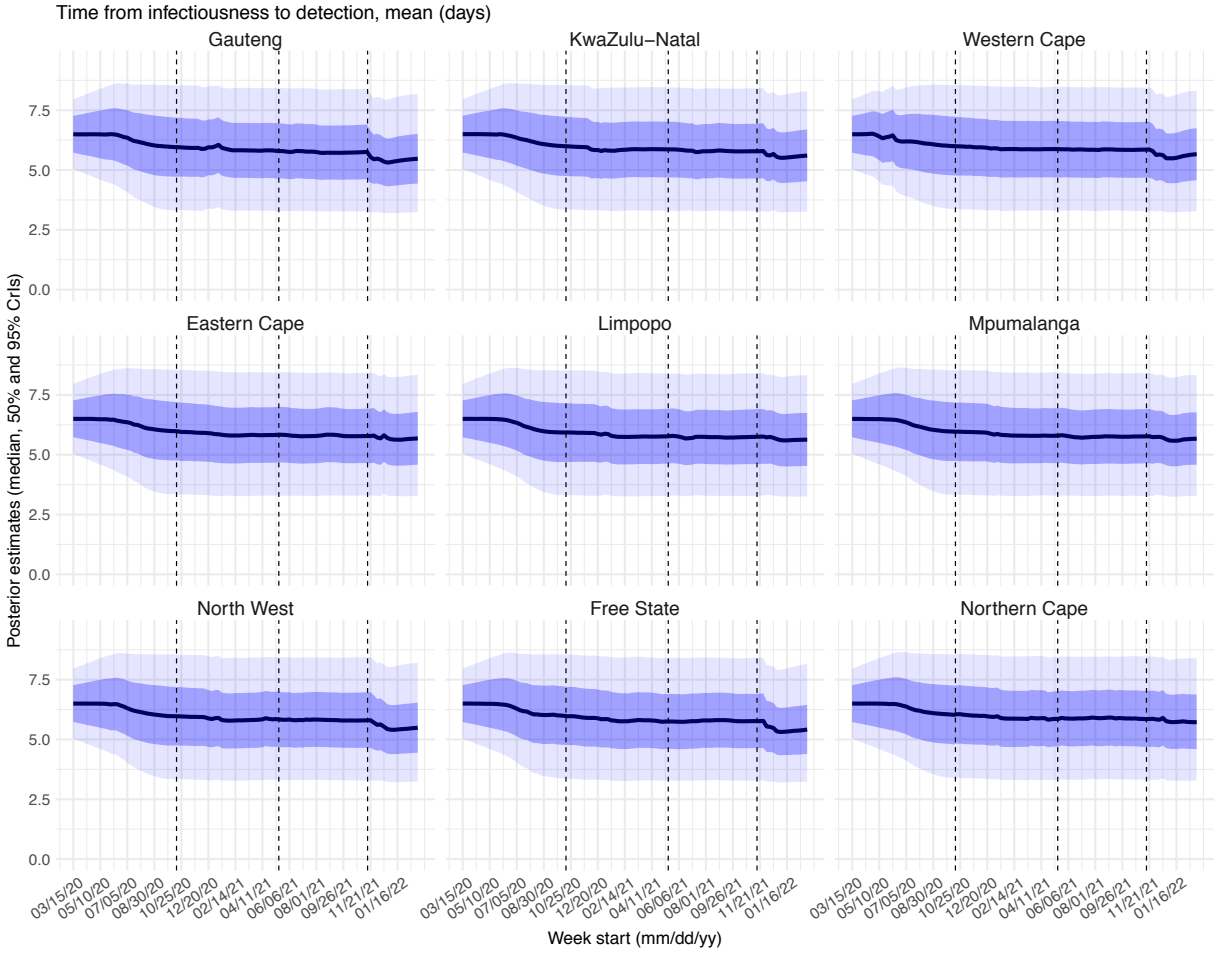

Fig S21. Posterior estimates for the standard deviation of time from infectiousness to detection ($T_{d,sd}$ in the observation model) by week. Thick black lines show the median, dark blue areas show the 50% CrIs, and light blue areas show the 95% CrIs. For reference, the dashed vertical black lines indicate three dates (mm/dd/yy), i.e., 10/15/20, 5/15/21, and 11/15/21, roughly the start of the Beta, Delta, and Omicron waves, respectively.

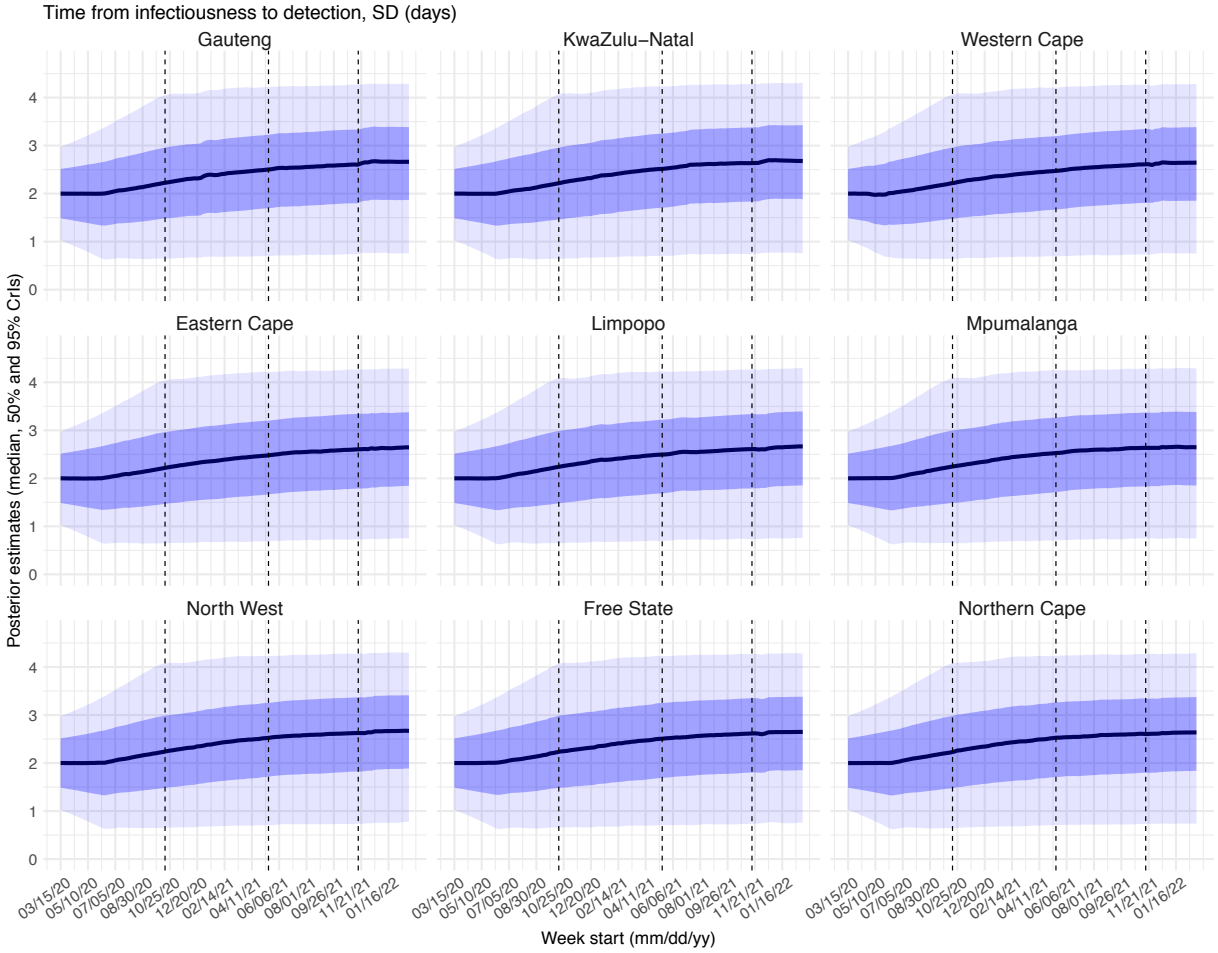

Fig S22. Posterior estimates for infection-detection rate (r_t in the observation model) by week. Thick black lines show the median, dark blue areas show the 50% CrIs, and light blue areas show the 95% CrIs. For reference, the dashed vertical black lines indicate three dates (mm/dd/yy), i.e., 10/15/20, 5/15/21, and 11/15/21, roughly the start of the Beta, Delta, and Omicron waves, respectively.

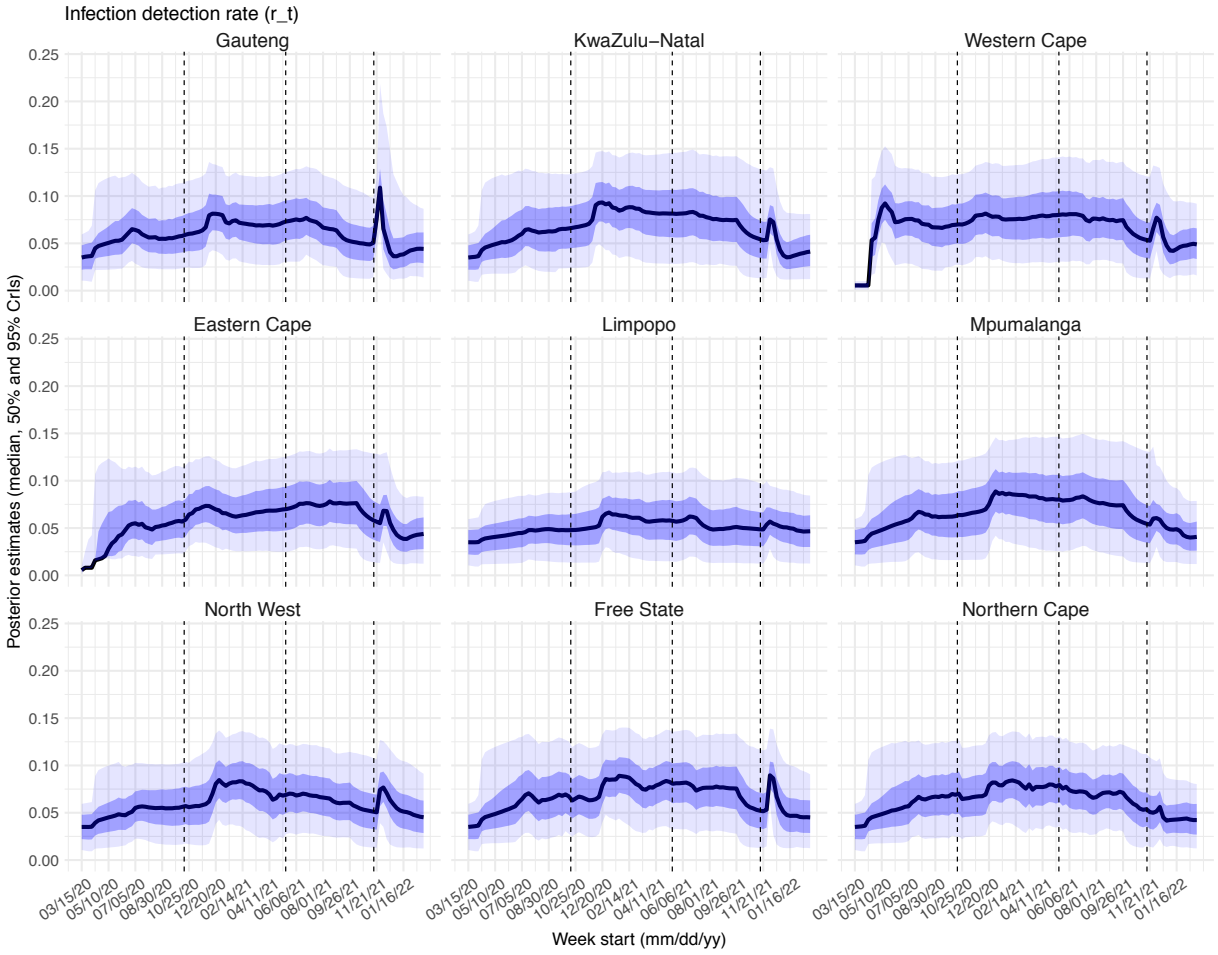

Fig S23. Posterior estimates for infection-fatality risk (IFR_t in the observation model) by week. Thick black lines show the median, dark blue areas show the 50% CrIs, and light blue areas show the 95% CrIs. For reference, the dashed vertical black lines indicate three dates (mm/dd/yy), i.e., 10/15/20, 5/15/21, and 11/15/21, roughly the start of the Beta, Delta, and Omicron waves, respectively.

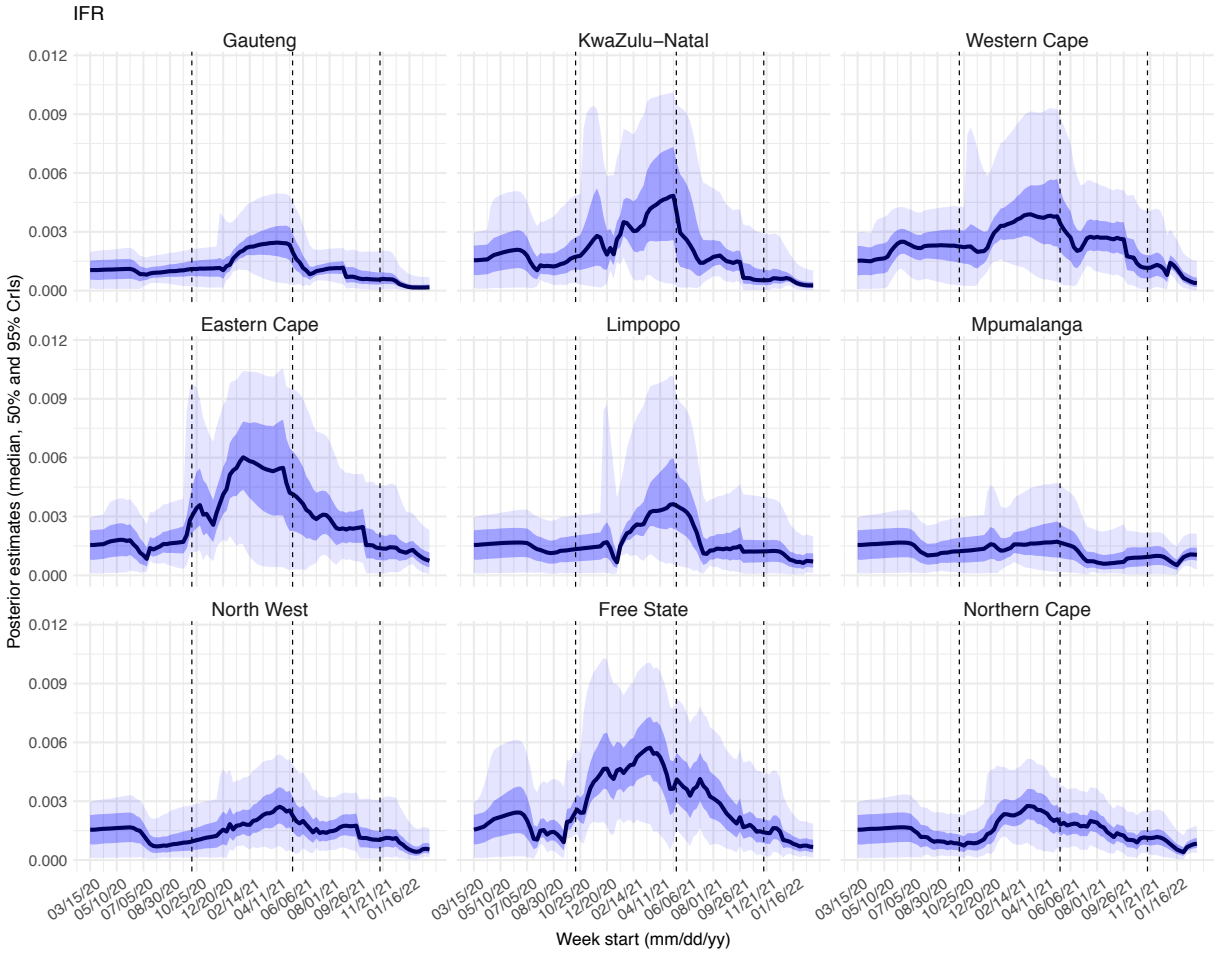

Table S1. Model estimated infection-detection rate during each wave. Numbers show the estimated percentage of infections (including asymptomatic and subclinical infections) documented as cases (mean and 95% CI in parentheses).

Province	Ancestral wave	Beta wave	Delta wave	Omicron wave
Gauteng	4.59 (2.62, 9.77)	6.18 (3.29, 11.11)	6.27 (3.44, 12.39)	4.16 (2.46, 9.72)
KwaZulu-Natal	4.33 (2.01, 11.02)	7.4 (3.89, 13.67)	5.69 (2.69, 12.34)	3.25 (1.84, 7.81)
Western Cape	5.62 (3, 10.93)	7.1 (3.99, 12.78)	6.83 (3.71, 13.08)	4.26 (2.49, 9.37)
Eastern Cape	3.79 (1.98, 9.39)	6.1 (3.35, 11.27)	5.58 (2.63, 11.52)	2.91 (1.4, 7.99)
Limpopo	2.13 (0.79, 6.46)	4.57 (1.89, 10.01)	3.4 (1.53, 9.3)	2.9 (1.2, 7.55)
Mpumalanga	3.42 (1.42, 9.1)	6.28 (2.85, 12.51)	5.71 (2.58, 12.96)	3.13 (1.54, 7.24)
North West	3.37 (1.62, 7.88)	5.79 (2.77, 11.14)	5.26 (2.8, 10.8)	3.73 (1.78, 8.62)
Free State	5.02 (2.83, 10.63)	6.69 (3.69, 11.97)	6.5 (3.16, 13.23)	4.03 (2.12, 8.95)
Northern Cape	4.96 (2.75, 10.34)	6.49 (3.72, 11.44)	6.69 (3.74, 12.32)	3.71 (1.97, 8.21)

Table S2. Model estimated attack rate during each wave. Numbers show estimated cumulative infection numbers, expressed as percentage of population size (mean and 95% CI in parentheses).

Province	Ancestral wave	Beta wave	Delta wave	Omicron wave
Gauteng	32.83 (15.42, 57.59)	21.87 (12.16, 41.13)	49.82 (25.22, 90.79)	44.49 (19.01, 75.3)
KwaZulu-Natal	24.06 (9.45, 51.91)	26.36 (14.28, 50.18)	27.15 (12.52, 57.39)	38.11 (15.87, 67.56)
Western Cape	28.44 (14.61, 53.17)	37.09 (20.61, 66.04)	47.29 (24.68, 87.1)	44.1 (20.02, 75.4)
Eastern Cape	32.85 (13.27, 62.95)	27.44 (14.86, 49.95)	25.59 (12.4, 54.34)	26.38 (9.59, 54.69)
Limpopo	13.78 (4.55, 37.21)	17.12 (7.82, 41.41)	28.22 (10.33, 62.74)	18.62 (7.15, 45.01)
Mpumalanga	18.99 (7.14, 45.83)	17.33 (8.7, 38.21)	27.18 (11.97, 60.14)	27.67 (11.96, 56.13)
North West	24.57 (10.51, 51.09)	16.04 (8.34, 33.49)	37.21 (18.13, 70.02)	26.17 (11.33, 54.71)
Free State	39.31 (18.54, 69.57)	24.23 (13.54, 43.92)	30.85 (15.16, 63.38)	32.79 (14.76, 62.32)
Northern Cape	34.92 (16.77, 63.13)	26.98 (15.3, 47.09)	55.59 (30.18, 99.32)	36.87 (16.65, 69.34)

Table S3. Model estimated infection-fatality risk during each wave. Numbers are percentages (%; mean and 95% CI in parentheses). Note that these estimates were based on reported COVID-19 deaths and may be biased due to likely under-reporting of COVID-19 deaths. In addition, due to data irregularities, we computed the IFR using two methods. Estimates per Method 1 are the ratio of the total reported COVID-19 related deaths to the model-estimated cumulative infection rate during each wave. Estimates per Method 2 are the weighted average of the weekly IFR estimates during each wave. See details in Section 1 of the Supplemental text.

Province	Ancestral wave	Beta wave	Delta wave	Omicron wave
Estimates per Method 1 (i.e., use reported COVID-19 deaths as the numerator):				
Gauteng	0.09 (0.05, 0.2)	0.19 (0.1, 0.33)	0.11 (0.06, 0.21)	0.03 (0.02, 0.06)
KwaZulu-Natal	0.09 (0.04, 0.24)	0.27 (0.14, 0.49)	0.14 (0.06, 0.29)	0.03 (0.02, 0.08)
Western Cape	0.21 (0.11, 0.41)	0.3 (0.17, 0.54)	0.25 (0.14, 0.48)	0.06 (0.04, 0.14)
Eastern Cape	0.11 (0.06, 0.27)	0.5 (0.27, 0.91)	0.2 (0.1, 0.42)	0.08 (0.04, 0.22)
Limpopo	0.06 (0.02, 0.17)	0.18 (0.08, 0.4)	0.1 (0.04, 0.27)	0.05 (0.02, 0.12)
Mpumalanga	0.07 (0.03, 0.18)	0.1 (0.05, 0.2)	0.04 (0.02, 0.1)	0.21 (0.11, 0.5)
North West	0.05 (0.02, 0.11)	0.21 (0.1, 0.4)	0.16 (0.08, 0.32)	0.05 (0.03, 0.12)
Free State	0.13 (0.08, 0.28)	0.42 (0.23, 0.75)	0.26 (0.13, 0.52)	0.09 (0.05, 0.2)
Northern Cape	0.06 (0.03, 0.13)	0.21 (0.12, 0.37)	0.17 (0.1, 0.32)	0.22 (0.12, 0.48)
Estimates per Method 2 (i.e., weighted average of weekly IFR estimates):				
Gauteng	0.09 (0.02, 0.18)	0.18 (0.05, 0.38)	0.12 (0.04, 0.25)	0.06 (0.01, 0.16)
KwaZulu-Natal	0.16 (0.02, 0.4)	0.28 (0.07, 0.69)	0.21 (0.06, 0.55)	0.08 (0.01, 0.23)
Western Cape	0.23 (0.06, 0.4)	0.3 (0.11, 0.68)	0.28 (0.09, 0.56)	0.13 (0.02, 0.32)
Eastern Cape	0.15 (0.03, 0.33)	0.39 (0.13, 0.8)	0.3 (0.07, 0.65)	0.15 (0.02, 0.39)
Limpopo	0.15 (0.01, 0.31)	0.19 (0.02, 0.6)	0.2 (0.03, 0.54)	0.11 (0.01, 0.31)
Mpumalanga	0.14 (0.01, 0.29)	0.16 (0.02, 0.39)	0.1 (0.01, 0.29)	0.1 (0.01, 0.2)
North West	0.12 (0.01, 0.27)	0.21 (0.04, 0.45)	0.17 (0.05, 0.37)	0.1 (0.01, 0.26)
Free State	0.18 (0.05, 0.45)	0.46 (0.15, 0.87)	0.32 (0.09, 0.65)	0.14 (0.03, 0.34)
Northern Cape	0.12 (0.02, 0.27)	0.22 (0.07, 0.44)	0.18 (0.05, 0.34)	0.1 (0.02, 0.22)

Table S4. Example estimation of reinfection rates. As an example, to compute reinfection rates, assume Beta is estimated θ_{beta} = 65% immune erosive, Delta is estimated θ_{delta} = 40% immune erosive, and Omicron BA.1 is estimated $\theta_{omicron}$ = 65% immune erosive, relative to the combined immunity accumulated until the rise of each of these variants (2nd column); and the attack rates (3rd column) are $c_1 = z_1$ = 30%, z_2 = 20%, z_3 = 50%, and z_4 = 40% during the ancestral, Beta, Delta, and Omicron BA.1 waves, respectively. Note these numbers roughly align with our estimates for Gauteng. The cumulative percentage of the population ever infected (including reinfections; 4th column), the percentage of reinfection during each VOC wave among the entire population (5th column) or among those infected by that variant (6th column) can be computed using the approach described in the supplemental text, sub-section "A proposed approach to compute reinfection rates using the model-inference estimates."

Variant	Immune erosion, θ	Attack rate, *z*	Cumulative % ever infected, *c*	Percentage reinfection this wave, among	
				entire population, η'	those infected this wave, η
Ancestral	-	30.0%	30.0%	-	-
Beta	65.0%	20.0%	45.6%	4.4%	21.8%
Delta	40.0%	50.0%	83.1%	12.6%	25.1%
Omicron (BA.1)	65.0%	40.0%	92.6%	30.5%	76.1%

Table S5. Prior ranges for the parameters used in the model-inference system. All initial values are drawn from uniform distributions using Latin Hypercube Sampling.

Parameter/ variable	Symbol	Prior range	Source/rationale
Initial exposed	$E(t=0)$	1 – 500 times of reported cases during the Week of March 15, 2020 for Western Cape and Eastern Cape; 1 – 10 times of reported cases during the Week of March 15, 2020, for other provinces	Low infection-detection rate in first weeks; earlier and higher case numbers reported in Western Cape and Eastern Cape than other provinces.
Initial infectious	$I(t=0)$	Same as for $E(t=0)$	
Initial susceptible	$S(t=0)$	99 – 100% of the population	Almost everyone is susceptible initially
Population size	N	N/A	Based on population data from COVID19ZA (main text ref 24)
Variant-specific transmission rate	β	For all provinces, starting from U[0.4, 0.7] at time 0 and allowed to increase over time using space re-probing(1) with values drawn from U[0.5, 0.9] during the Beta wave, U[0.7, 1.25] during the Delta wave, and U[0.7, 1.3] during the Omicron wave.	For the initial range at model initialization, based on R_0 estimates of around 1.5-4 for SARS-CoV-2.(2-4) For the Beta, Delta and Omicron variants, we use large bounds for space re-probing (SR)(1) to explore the parameter state space and enable estimation of changes in transmissibility due to the new variants. Note that SR is only applied to 3-10% of the ensemble members and β can migrate outside either the initial range or the SR ranges during EAKF update.
Scaling of effectiveness of NPI	e	[0.5, 1.5], for all provinces	Around 1, with a large bound to be flexible.

Latency period	Z	[2, 5] days, for all provinces	Incubation period: 5.2 days (95% CI: 4.1, 7)(2); latency period is likely shorter than the incubation period
Infectious period	D	[2, 5] days, for all provinces	Time from symptom onset to hospitalization: 3.8 days (95% CI: 0, 12.0) in China,(5) plus 1-2 days viral shedding before symptom onset. We did not distinguish symptomatic/asymptomatic infections.
Immunity period	L	[730, 1095] days, for all provinces	Assuming immunity lasts for 2-3 years
Mean of time from viral shedding to diagnosis	T_m	[5, 8] days, for all provinces	From a few days to a week from symptom onset to diagnosis/reporting,(5) plus 1-2 days of viral shedding (being infectious) before symptom onset.
Standard deviation (SD) of time from viral shedding to diagnosis	T_{sd}	[1, 3] days, for all provinces	To allow variation in time to diagnosis/reporting
Infection-detection rate	r	Starting from U[0.001, 0.01] at time 0 for Western Cape and Eastern Cape as these two provinces had earlier and higher case numbers during March – April 2020 than other provinces, suggesting lower detection rate at the time; for the rest starting from U[0.01, 0.06]. For all provinces,	Large uncertainties; therefore, in general we use large prior bounds and large bounds for space re-probing (SR). Note that SR is only applied to 3-10% of the ensemble members and r can migrate

	allowed *r* to increase over time using space re-probing (1) with values drawn from uniform distributions with ranges between roughly 0.01 to 0.12.	outside either the initial range or the SR ranges during EAKF update.
Infection fatality risk (IFR)	For Gauteng: starting from [0.0001, 0.002] at time 0 and allowed to change over time using space re-probing(1) with values drawn from U[0.0001, 0.005] during 12/13/2020 – 5/15/21 (due to Beta), U[0.0001, 0.002] during the Delta wave, and U[0.00001, 0.00075] starting 9/1/21 (Omicron wave). For KwaZulu-Natal: starting from U[0.0001, 0.003] at time 0 and allowed to change over time using space re-probing (1) with values drawn from U[0.0001, 0.005] during 4/19/20 –10/31/20 (ancestral wave), U[0.0001, 0.01] during 11/1/20 – 5/15/21 (Beta wave), U[0.0001, 0.002] during the Delta wave, and U[0.00001, 0.00075] starting 10/1/21 (Omicron wave). For Western Cape: starting from U[0.00001, 0.003] at time 0 and allowed to change over time using space re-probing (1) with values drawn from U[0.00001, 0.0004] during 4/19/20 – 10/31/20 (ancestral wave), U[0.00001, 0.01] during 11/1/20 – 5/15/21 (Beta wave), U[0.00001, 0.005] during 5/16/21 – 9/30/21 (Delta wave) and U[0.00001, 0.002] starting 10/1/21 (Omicron wave). For Eastern Cape: starting from U[0.0001, 0.003] at time 0 and allowed to change over time using space re-probing(1) with values drawn from U[0.0001, 0.004] during 4/19/20 – 9/30/20 (Ancestral wave), U[0.0001, 0.01] during 10/1/20 – 40/30/21 (Beta wave), [0.0001, 0.005] during the Delta wave, and U[0.00001, 0.002] or starting 10/16/21 (Omicron wave).	Based on previous estimates(6) but extend to have wider ranges. Note that SR is only applied to 3-10% of the ensemble members and IFR can migrate outside either the initial range or the SR ranges during EAKF update. Western Cape had earlier and higher case numbers during March – April 2020 than other provinces, suggesting lower detection rate at the time. Initial mortality rate in Gauteng was relatively low because initial infections occurred mainly among middle-aged, returning holiday makers.(7) Earlier spread of Beta in Eastern Cape, KwaZulu-Natal, and Northern Cape, higher numbers of deaths per capita reported. Free State reported higher number of deaths per capita.

	For Limpopo and Mpumalanga: starting from U[0.0001, 0.003] at time 0 and allowed to change over time using space re-probing (1) with values drawn from U[0.0001, 0.01] during the Beta wave, U[0.0001, 0.005] during the Delta wave, U[0.00001, .002] for the Omicron wave. For Free State: starting from U[0.0001, 0.003] at time 0 and allowed to change over time using space re-probing (1) with values drawn from U[0.0001, 0.006] during 3/16/20 – 10/31/20, U[0.0001, 0.01] during the Beta wave, U[0.0001, 0.008] during the Delta wave, and U[0.00001, 0.002] starting 10/1/21 (Omicron wave). For North West and Northern Cape: starting from U[0.0001, 0.003] at time 0 and allowed to change over time using space re-probing (1) with values drawn from U[0.0001, 0.005] during the Beta wave, U[0.0001, 0.003] during the Delta wave, and U[0.00001, 0.0015] starting 10/1/21 (Omicron wave).

References including in Table S5:

1. Yang W & Shaman J (2014) A simple modification for improving inference of non-linear dynamical systems. *arXiv*:1403.6804.
2. Li Q*, et al.* (2020) Early Transmission Dynamics in Wuhan, China, of Novel Coronavirus–Infected Pneumonia. *New Engl J Med*.
3. Wu JT, Leung K, & Leung GM (2020) Nowcasting and forecasting the potential domestic and international spread of the 2019-nCoV outbreak originating in Wuhan, China: a modelling study. *Lancet* 395(10225):689-697.
4. Li R*, et al.* (2020) Substantial undocumented infection facilitates the rapid dissemination of novel coronavirus (SARS-CoV-2). *Science* 368(6490):489-493.
5. Zhang J*, et al.* (2020) Evolving epidemiology and transmission dynamics of coronavirus disease 2019 outside Hubei province, China: a descriptive and modelling study. *The Lancet. Infectious diseases* 20(7):793-802.
6. Verity R*, et al.* (2020) Estimates of the severity of coronavirus disease 2019: a model-based analysis. *The Lancet. Infectious diseases* 20(6):669-677.
7. Giandhari J*, et al.* (2021) Early transmission of SARS-CoV-2 in South Africa: An epidemiological and phylogenetic report. *Int J Infect Dis* 103:234-241.

Table S6. Approximate epidemic timing (mm/dd/yy) for each wave in each province, used in the study. Note 3/5/22 is the last date of the study period.

Province	Variant	Start date	End date
Gauteng	Ancestral	3/15/20	10/31/20
Gauteng	Beta	11/1/20	5/15/21
Gauteng	Delta	5/16/21	8/31/21
Gauteng	Omicron	9/1/21	3/5/22
KwaZulu-Natal	Ancestral	3/15/20	9/15/20
KwaZulu-Natal	Beta	9/16/20	5/15/21
KwaZulu-Natal	Delta	5/16/21	9/30/21
KwaZulu-Natal	Omicron	10/1/21	3/5/22
Western Cape	Ancestral	3/15/20	9/15/20
Western Cape	Beta	9/16/20	5/15/21
Western Cape	Delta	5/16/21	9/30/21
Western Cape	Omicron	10/1/21	3/5/22
Eastern Cape	Ancestral	3/15/20	8/15/20
Eastern Cape	Beta	8/16/20	4/30/21
Eastern Cape	Delta	5/1/21	10/15/21
Eastern Cape	Omicron	10/16/21	3/5/22
Limpopo	Ancestral	3/15/20	10/31/20
Limpopo	Beta	11/1/20	5/15/21
Limpopo	Delta	5/16/21	9/30/21
Limpopo	Omicron	10/1/21	3/5/22
Mpumalanga	Ancestral	3/15/20	10/31/20
Mpumalanga	Beta	11/1/20	5/15/21
Mpumalanga	Delta	5/16/21	9/30/21
Mpumalanga	Omicron	10/1/21	3/5/22
North West	Ancestral	3/15/20	10/31/20
North West	Beta	11/1/20	5/15/21
North West	Delta	5/16/21	9/30/21
North West	Omicron	10/1/21	3/5/22
Free State	Ancestral	3/15/20	10/31/20
Free State	Beta	11/1/20	5/31/21
Free State	Delta	6/1/21	9/30/21
Free State	Omicron	10/1/21	3/5/22
Northern Cape	Ancestral	3/15/20	10/31/20
Northern Cape	Beta	11/1/20	5/15/21
Northern Cape	Delta	5/16/21	9/30/21
Northern Cape	Omicron	10/1/21	3/5/22